FREQUENCY SPLITTING WITH TWO DIMENSIONAL TRIANGULAR PHOTONIC CRYSTAL

A Thesis Submitted to
the Graduate School of Engineering and Sciences of
İzmir Institute of Technology
in Partial Fulfillment of the Requirements for the Degree of

MASTER OF SCIENCE

in Physics

by
Adem Enes Erol

November 2009
İZMİR

We approve the thesis of **Adem Enes Erol**

Asst. Prof. H. Sami Sözüer
Supervisor

Prof. Orhan Öztürk
Committee Member

Assoc. Prof. M. Salih Dinleyici
Committee Member

2 October 2009

Prof. Durmuş Ali DEMİR
Head of the Department of Physics

Assoc. Prof. Talat YALÇIN
Dean of the Graduate School of
Engineering and Sciences

ACKNOWLEDGMENTS

I would like to thank my family for their financial and emotional aid during my days as a graduate student. If it weren't for their generous help, this thesis would not have been possible. I am very grateful to my supervisor, Asst. Prof. Dr. H. Sami Sözüer, for his powerful guidence and fruitful discussions. I would also like to thank my group friends, H. Duygu Şengün and Neslihan Çileli, for their motivating words and valuable discussions. And I thank to all my friends at the Institute for all their help and friendship. Finally, I acknowledge all smiling people in the world for making the world a more livable.

ABSTRACT

FREQUENCY SPLITTING WITH TWO DIMENSIONAL TRIANGULAR PHOTONIC CRYSTAL

Photonic crystals are periodically arranged dielectric materials. If the periodicity is broken along a line, i.e. a line defect is formed, then the line defect can behave like a waveguide. In this thesis, a frequency splitting device for electromagnetic waves is designed and tested theoretically using line defect waveguides. The theoretical design of the waveguides is accomplished using the plane wave expansion and the supercell method. The testing is done by the finite difference time domain method.

Frequency mixing and splitting, or multiplexers and demultiplexers as they are known in industry, for electromagnetic waves are important since they lead to a multiplication in capacity for optical communications. Multiplexers and demultiplexers have been in use for a long time. However, designing photonic crystal multiplexers has a history of about ten years. In this thesis, a new photonic crystal demultiplexer design is suggested using photonic crystal line defect waveguides.

ÖZET

İKİ BOYUTLU ÜÇGEN ÖRGÜLÜ FOTONİK KRİSTAL İLE FREKANS AYIRMA

Fotonik kristaller periyodik olarak dizilmiş dielektrik malzemelerdir. Bu periyodiklik bir doğru boyunca bozulunca, yani çizgisel bir kusur meydana getirilince, bu çizgisel kusur dalga kılavuzu gibi davranabilir. Bu tezde, çizgisel kusurlu dalga kılavuzları kullanılarak, elektromagnetik dalgalar için frekans ayırma aygıtı teorik olarak tasarlandı ve sınandı. Bu dalga kılavuzlarını teorik olarak tasarlama düzlem dalga açılım ve süperhücre yöntemleriyle yapıldı. Teorik sınamada ise sonlu farklar zaman alanı yöntemi kullanıldı.

Elektromagnetik dalgalar için frekansları birleştirme ve ayırma aygıtları önemliler çünkü bunlar optik haberleşmede bilgi aktarım kapasitesini katlamayı sağlarlar. Bu aygıtlar uzun zamandır kullanılıyorlar. Ama fotonik kristallerle tasarımları on senelik bir geçmişe sahip. Bu tezde, fotonik kristal çizgisel kusurlu dalga kılavuzlarıyla yapılan yeni bir fotonik kristal frekans ayırma aygıtı öneriliyor.

TABLE OF CONTENTS

LIST OF FIGURES

CHAPTER 1

INTRODUCTION

The title of the thesis immediately brings up two questions to the mind of the reader unfamiliar with the subject matter. The first question: *What is a photonic crystal?* The question will be answered in the first chapter. We will also briefly mention some applications of photonic crystals in general.

The second question is, *What does "frequency splitting" mean?* We will attempt to answer this question in Section 1.3 and in Chapter 3 The heart of the thesis is Chapter 3, where our device for frequency splitting is discussed in detail.

How do we study photonic crystals? We used two methods for studying photonic crystals. One of them is the finite difference time domain (FDTD) method widely used in a variety of problems in computational electrodynamics. The other one is the plane wave expansion method and supercell method for theoretical prediction, before computational modeling. These methods will be explained in Chapter 2.

To understand the material in this thesis, the reader needs to be familiar with basic **electromagnetic theory** (Griffiths 1999), basic **solid state physics** (Kittel 1996) and a little mathematics, especially **Fourier analysis** and **eigenvalue problems** (Arfken and Weber 2005). *What about quantum mechanics?* As we will see in Section 3.6, the scale of the problem we are studying is $\sim 1.5\mu m$, so we remain in the classical region. So we don't take into account any quantum mechanical effect in this thesis. All quantum mechanical effects are implicitly taken into account through the dielectric constant of the material of which the photonic crystal is made.

1.1. Photonic Crystals

What are photonic crystals? As is well-known, a crystal is a material whose components (atoms, molecules, or ions) are arranged in an orderly repeating pattern extending in one, two, or three dimensions. Similarly, a photonic crystal (PhC) is a structure which

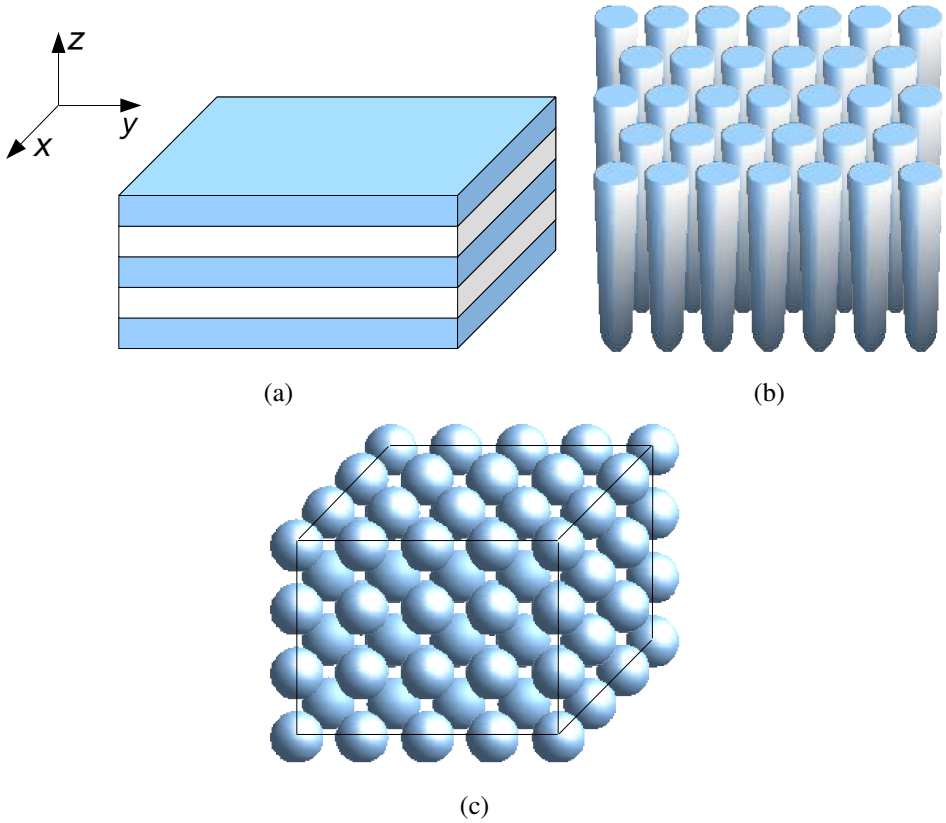

Figure 1.1. (a) A 1D photonic crystal, (b) a 2D photonic crystal, (c) a 3D photonic crystal.

is formed by periodically arranging materials with different dielectric constants, ϵ. A one-dimensional (1D) PhC is shown in Figure 1.1a. It is actually a multilayer film. The white and blue layers represent materials with different dielectric constants. Its periodicity is only along the z-axis, which is why this kind of PhCs is called one-dimensional PhCs.

An example of a second kind of PhC is shown in Figure 1.1b. This is a two-dimensional (2D) PhC, because it is periodic in the xy-plane only, with no variation of the dielectric constant along the z-axis. The rods and space represent materials with different dielectric constants. We will be concerned with only **2D PhCs** in this thesis.

Finally, if the periodicity of the PhC extends in all three dimensions, this kind of PhCs are called three-dimensional (3D) PhCs. An example of a 3D PhC is shown in Figure 1.1c. The spheres and space stand for materials with different dielectric constant again.

Which properties of PhCs make them desirable for optical device applications? The most important property of PhCs is the electromagnetic, or **photonic band gap**. A

photonic band gap is a region in the frequency spectrum, in which the propagation of EM waves with frequencies within the gap is strictly forbidden. The possibility of creating a photonic band gap with 3D periodic dielectric structures was suggested by (Yablonovitch 1987).

Another most important property is **strong localization of EM waves** in certain disordered dielectric superlattices. A disordered dielectric superlattice is a lattice with weak disordering of a periodic dielectric structure. Strong localization of EM waves may be achieved in defect regions. This idea was suggested by (John 1987). These properties make PhCs powerful tools for manipulation of EM waves.

1.2. Applications of Photonic Crystals

PhCs are powerful tools for manipulation of EM waves. *Then what are applications of PhCs with these significant properties?* One of the most researched applications is **photonic crystal fibers** which are a new class of optical waveguides. It is known that optical fibers play an important role in modern communications. A traditional optical fiber consists of a central core and a cladding which surrounds the core. Light is guided in the core along the optical fiber by total internal reflection since the core refractive index is higher than the cladding refractive index.

This next generation PhC fiber has a core and a cladding like conventional optical fiber, and it is made of a 2D periodic dielectric structure perpendicular to its axis. PhC fibers can be divided into two types. One is the index-guided PhC fibers first reported by (Knight, et al. 1996). Index-guided PhC fibers are similar to conventional optical fibers because the core effective refractive index is higher than the cladding effective refractive index. They can have a much higher dielectric contrast between the core and the cladding than conventional optical fibers leading to a greater strength of optical confinement. And they are useful for enhancing nonlinear effects and creating unusual dispersion phenomena (Joannopoulos, et al. 2008). In addition it is important that index-guided PhC fibers can remain single mode for a sufficiently large fiber lengths. This ability is known as endlessly single mode (Birks, et al. 1997).

The other type is photonic-bandgap fibers reported by (Knight, et al. 1998) and

(Cregan, et al. 1999). Photonic-bandgap fibers are different from traditional optical fibers. The core is air and the cladding effective refractive index is higher than that of air. So light guidance is explained by photonic band gap phenomena instead of total internal reflection. This minimizes the effects of losses, undesired nonlinearities and any other unwanted properties of the bulk materials (Joannopoulos, et al. 2008).

PhC fibers can be superior to classical fibers because they can have less attenuation, can transmit light with much higher optical power, have lower bending losses and can be used in an increasing number of applications in a broad range of areas (Russell 2006).

A challenge application: **Photonic integrated circuits**. It is known that electronic integrated circuits (IC) are made of transistors and transmission lines for electrons. In ICs information is transfered by electrons between transistors with transmission lines. In photonic ICs, information will be transfered by photons instead of electrons. However there are some difficulties for photonic ICs. The first problem in constructing photonic ICs is to guide EM waves without bending loss in waveguides. High transmission of EM waves through sharp bends was demonstrated theoretically by (Mekis, et al. 1996) and experimentally by (Lin, et al. 1998). Since the transmission lines have branches (or splitters) in ICs, the waveguides will have branches in photonic ICs as well. A branch for photonic ICs was simulated (Fan, et al. 2001) and another branch was realized experimentally (Lin, et al. 2002). The second problem in the way of a practical realization of photonic ICs is to make optical (or photonic) transistors. An all optical transistor is demonstrated by (Yanık, et al. 2003) theoretically with nonlinear PhCs. All optical bistable switch which is equivalent to optical transistor action is demonstrated by (Notomi, et al. 2005) experimentally. However combining all of those with low power requirements and high speed is still difficult for photonic ICs. More time is needed for realization of photonic ICs.

Other interesting topics with PhCs are microcavities (Villeneuve, et al. 1996, Foresi, et al. 1997), modification of spontaneous emission (Fan, et al. 1997), superprism phenomena (Hosaka, et al. 1998), reflector (Fink, et al. 1998), channel drop (Fan, et al. 1998), self-collimating phenomena (Kosaka, et al. 1999), negative refraction (Notomi 2000, Luo, et al. 2002), photonic crystal laser (Loncar, et al. 2002, Park, et al. 2004).

1.3. Wavelength Division Multiplexing

In fiber-optic communications, wavelength-division multiplexing is a technology which enables transmission of multiple optical signals on the same optical fiber simultaneously. The technology uses different wavelengths of laser light to carry different signals. This leads to a multiplication in capacity for communications. In this technology multiplexers are used for joining the signals together and demultiplexers are used for splitting the signals apart. *What does "frequency splitting" in the title of the thesis mean?* Frequency splitting means **demultiplexing** actually and our frequency splitting device is a **demultiplexer**.

Using a photonic crystal superprism, PhC demultiplexers were theoretically shown to be possible (Chung and Hong 2002, Momeni and Adibi 2003, Matsumoto, et al. 2005) and were experimentally realized (Momeni, et al. 2006). Multiplexing and demultiplexing using PhC waveguides were also theoretically shown to be possible (Chien, et al. 1999, Centeno, et al. 1999, Nelson, et al. 2000, Koshiba 2001, Sharkawy, et al. 2001, Smajic, et al. 2003). In this thesis we suggest a new PhC demultiplexer design using PhC waveguides.

CHAPTER 2

METHODOLOGY

2.1. Finite Difference Time Domain Method

Finite-difference time-domain (FDTD) is a popular computational electrodynamics modeling method (Yee 1966, Taflove and Brodwin 1975). *How does FDTD method work?* In this section we will answer this question.

Our starting point is Maxwell's equations. They are in Heaviside-Lorentz units

$$\nabla \cdot \mathbf{D} = \rho \tag{2.1}$$

$$\nabla \cdot \mathbf{B} = 0 \tag{2.2}$$

$$\nabla \times \mathbf{E} = -\frac{1}{c}\frac{\partial \mathbf{B}}{\partial t} \tag{2.3}$$

$$\nabla \times \mathbf{H} = \frac{\mathbf{J}}{c} + \frac{1}{c}\frac{\partial \mathbf{D}}{\partial t} \tag{2.4}$$

We assume that there is no charge density in a 2D PhC. However current density exists, because it is EM wave source for this modeling method. So

$$\nabla \cdot \mathbf{D} = 0 \tag{2.5}$$

$$\nabla \cdot \mathbf{B} = 0 \tag{2.6}$$

$$\nabla \times \mathbf{E} = -\frac{1}{c}\frac{\partial \mathbf{B}}{\partial t} \tag{2.7}$$

$$\nabla \times \mathbf{H} = \frac{\mathbf{J}}{c} + \frac{1}{c}\frac{\partial \mathbf{D}}{\partial t} \tag{2.8}$$

In scalar form Equation 2.7 is

$$\frac{\partial E_y}{\partial z} - \frac{\partial E_z}{\partial y} = \frac{1}{c}\frac{\partial B_x}{\partial t} \tag{2.9}$$
$$\frac{\partial E_z}{\partial x} - \frac{\partial E_x}{\partial z} = \frac{1}{c}\frac{\partial B_y}{\partial t} \tag{2.10}$$
$$\frac{\partial E_x}{\partial y} - \frac{\partial E_y}{\partial x} = \frac{1}{c}\frac{\partial B_z}{\partial t} \tag{2.11}$$

and Equation 2.8 is

$$\frac{\partial H_z}{\partial y} - \frac{\partial H_y}{\partial z} = \frac{J_x}{c} + \frac{1}{c}\frac{\partial D_x}{\partial t} \tag{2.12}$$
$$\frac{\partial H_x}{\partial z} - \frac{\partial H_z}{\partial x} = \frac{J_y}{c} + \frac{1}{c}\frac{\partial D_y}{\partial t} \tag{2.13}$$
$$\frac{\partial H_y}{\partial x} - \frac{\partial H_x}{\partial y} = \frac{J_z}{c} + \frac{1}{c}\frac{\partial D_z}{\partial t} \tag{2.14}$$

For simplicity, we focus our analysis on two dimension. So let's take

$$D_x = D_y = H_z = J_x = J_y = 0 \tag{2.15}$$

Then Equation 2.7-2.8 can be written

$$-\frac{\partial E_z}{\partial y} = \frac{1}{c}\frac{\partial B_x}{\partial t} \tag{2.16}$$
$$\frac{\partial E_z}{\partial x} = \frac{1}{c}\frac{\partial B_y}{\partial t} \tag{2.17}$$
$$\frac{\partial H_y}{\partial x} - \frac{\partial H_x}{\partial y} = \frac{J_z}{c} + \frac{1}{c}\frac{\partial D_z}{\partial t} \tag{2.18}$$

Using $\mathbf{D} = \epsilon\mathbf{E}$ and $\mathbf{B} = \mu\mathbf{H}$ equations in Heaviside-Lorentz units again, Equation 2.16-2.18 can be written

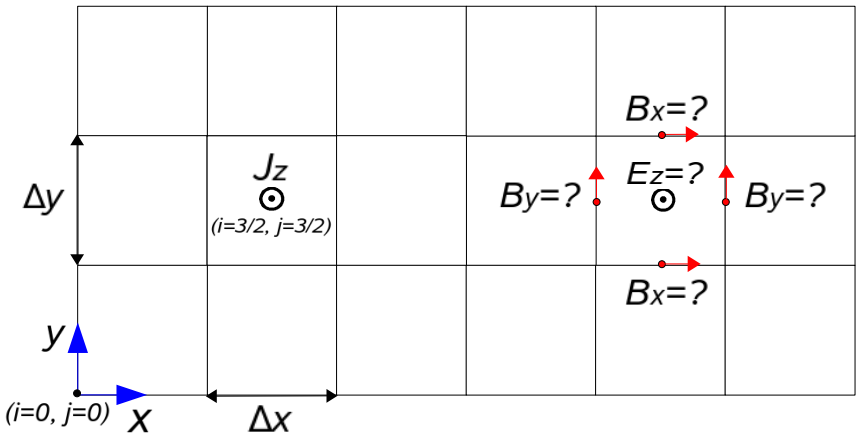

Figure 2.1. A Yee lattice in 2D. An exercise for FDTD method.

$$-\frac{\partial E_z}{\partial y} = \frac{\mu}{c}\frac{\partial H_x}{\partial t} \tag{2.19}$$

$$\frac{\partial E_z}{\partial x} = \frac{\mu}{c}\frac{\partial H_y}{\partial t} \tag{2.20}$$

$$\frac{\partial H_y}{\partial x} - \frac{\partial H_x}{\partial y} = \frac{J_z}{c} + \frac{\epsilon}{c}\frac{\partial E_z}{\partial t} \tag{2.21}$$

$\partial x, \partial y$ and ∂t are **infinitesimal differences** in Eqs. 2.19-2.21. If these infinitesimal differences are changed to **finite differences**, Eqs. 2.19-2.21 can are written

$$-\frac{\Delta E_z}{\Delta y} \approx \frac{\mu}{c}\frac{\Delta H_x}{\Delta t} \tag{2.22}$$

$$\frac{\Delta E_z}{\Delta x} \approx \frac{\mu}{c}\frac{\Delta H_y}{\Delta t} \tag{2.23}$$

$$\frac{\Delta H_y}{\Delta x} - \frac{\Delta H_x}{\Delta y} \approx \frac{J_z}{c} + \frac{\epsilon}{c}\frac{\Delta E_z}{\Delta t} \tag{2.24}$$

In Figure 2.1 there is a two dimensional discretized space. The space is diveded to 18 equal parts. This scheme is known as a **Yee lattice** (Yee 1966). Using the Yee lattice, Eqs. 2.22-2.24 can be written

$$-\frac{E_z^{k+\frac{1}{2}}(i+\frac{1}{2},j+\frac{1}{2})-E_z^{k+\frac{1}{2}}(i+\frac{1}{2},j-\frac{1}{2})}{\Delta y} \approx \frac{\mu(i+\frac{1}{2},j)}{c}\frac{H_x^{k+1}(i+\frac{1}{2},j)-H_x^{k}(i+\frac{1}{2},j)}{\Delta t} \quad (2.25)$$

$$\frac{E_z^{k+\frac{1}{2}}(i+\frac{1}{2},j+\frac{1}{2})-E_z^{k+\frac{1}{2}}(i-\frac{1}{2},j+\frac{1}{2})}{\Delta x} \approx \frac{\mu(i,j+\frac{1}{2})}{c}\frac{H_y^{k+1}(i,j+\frac{1}{2})-H_y^{k}(i,j+\frac{1}{2})}{\Delta t} \quad (2.26)$$

$$\frac{H_y^k(i+1,j+\frac{1}{2})-H_y^k(i,j+\frac{1}{2})}{\Delta x}-\frac{H_x^k(i+\frac{1}{2},j+1)-H_x^k(i+\frac{1}{2},j)}{\Delta y} \approx \frac{J_z^k(i+\frac{1}{2},j+\frac{1}{2})}{c}+\frac{\epsilon(i+\frac{1}{2},j+\frac{1}{2})}{c}\frac{E_z^{k+\frac{1}{2}}(i+\frac{1}{2},j+\frac{1}{2})-E_z^{k-\frac{1}{2}}(i+\frac{1}{2},j+\frac{1}{2})}{\Delta t} \quad (2.27)$$

where we take $A^k(i,j) = A(i\Delta x, j\Delta y, k\Delta t)$ and $i,j,k \in \mathbb{Z}$. These equations can be written as a **recursion equations** form for the FDTD method

$$E_z^{k+\frac{1}{2}}(i+\frac{1}{2},j+\frac{1}{2}) \approx E_z^{k-\frac{1}{2}}(i+\frac{1}{2},j+\frac{1}{2})-\frac{\Delta t J_z^k(i+\frac{1}{2},j+\frac{1}{2})}{\epsilon(i+\frac{1}{2},j+\frac{1}{2})} + \frac{c\Delta t}{\Delta x}\frac{H_y^k(i+1,j+\frac{1}{2})-H_y^k(i,j+\frac{1}{2})}{\epsilon(i+\frac{1}{2},j+\frac{1}{2})} - \frac{c\Delta t}{\Delta y}\frac{H_x^k(i+\frac{1}{2},j+1)-H_x^k(i+\frac{1}{2},j)}{\epsilon(i+\frac{1}{2},j+\frac{1}{2})} \quad (2.28)$$

$$H_x^{k+1}(i+\frac{1}{2},j) \approx H_x^k(i+\frac{1}{2},j) - \frac{c\Delta t}{\Delta y}\frac{E_z^{k+\frac{1}{2}}(i+\frac{1}{2},j+\frac{1}{2})-E_z^{k+\frac{1}{2}}(i+\frac{1}{2},j-\frac{1}{2})}{\mu(i+\frac{1}{2},j)} \quad (2.29)$$

$$H_y^{k+1}(i,j+\frac{1}{2}) \approx H_y^k(i,j+\frac{1}{2}) + \frac{c\Delta t}{\Delta x}\frac{E_z^{k+\frac{1}{2}}(i+\frac{1}{2},j+\frac{1}{2})-E_z^{k+\frac{1}{2}}(i-\frac{1}{2},j+\frac{1}{2})}{\mu(i,j+\frac{1}{2})} \quad (2.30)$$

With Eqs. 2.28-2.30, values of vector field components (E_z, B_x or B_y) at any lattice point and at any time can be found depending on their initial or previous values.

2.1.1. An Exercise for FDTD Method

How do we use Eqs. 2.28-2.30? To understand how to use Eqs. 2.28-2.30 for finding the values of the vector field components at any lattice point and any time, let's make a simple example.

In Figure 2.1 at $(i = 3/2, j = 3/2)$ Yee lattice point there is a current density J_z. When $k < 0$ which means $t = k\Delta t < 0$, the initial condition is

$$J_z^{k<0}(3/2, 3/2) = 0 \tag{2.31}$$

and when $k \leq 0$,

$$E_z^{k\leq 0}(i, j) = B_x^{k\leq 0}(i, j) = B_y^{k\leq 0}(i, j) = 0. \tag{2.32}$$

When $k \geq 0$, let's take

$$J_z^0(3/2, 3/2) = J_z^{k>0}(3/2, 3/2) \neq 0. \tag{2.33}$$

J_z changes with time at $k = 0$. As a result EM wave is created. Using Equation 2.30, one can find

$$E_z^{\frac{1}{2}}(\frac{3}{2}, \frac{3}{2}) \approx -\frac{\Delta t}{\epsilon(\frac{3}{2}, \frac{3}{2})} J_z^0(\frac{3}{2}, \frac{3}{2}) \tag{2.34}$$

Using Equation 2.28-2.29, one can achieve

$$H_y^1(2,\frac{3}{2}) \approx -\frac{c\Delta t}{\mu(2,\frac{3}{2})\Delta x} E_z^{\frac{1}{2}}(\frac{3}{2},\frac{3}{2}) \tag{2.35}$$

$$H_y^1(1,\frac{3}{2}) \approx \frac{c\Delta t}{\mu(1,\frac{3}{2})\Delta x} E_z^{\frac{1}{2}}(\frac{3}{2},\frac{3}{2}) \tag{2.36}$$

$$H_x^1(\frac{3}{2},2) \approx -\frac{c\Delta t}{\mu(\frac{3}{2},2)\Delta y} E_z^{\frac{1}{2}}(\frac{3}{2},\frac{3}{2}) \tag{2.37}$$

$$H_x^1(\frac{3}{2},1) \approx \frac{c\Delta t}{\mu(\frac{3}{2},1)\Delta y} E_z^{\frac{1}{2}}(\frac{3}{2},\frac{3}{2}) \tag{2.38}$$

When one continues the calculation with same way, the computation of the vector fields can be proceeded easily

2.1.2. Geometric Structures in a Yee lattice

It is understood that a Yee lattice consists of several square parts. *Then how can we insert any sort of geometric structure into a Yee lattice?* Actually **rule** is very easy. Each part of a Yee lattice are given an avarage dielectric constant value according to the shape of the geometric object. To understand very well, let's insert a triangular object into the Yee lattice in Figure 2.2.

The triangular structure is on six Yee lattice parts. Three of them consist of air and dielectric material ($\epsilon_{diel} = 9$) fairly. According to the rule, their dielectric constant values are taken 5. So our triangular object looks in Figure 2.2. With this rule any kind of structure which we study can be inserted in a simulation space (see Figure 2.3.

To close more real results, the Yee lattice should be divided more that 18 parts. However it cannot be an enormous number because of computer technology limits. Before starting a computation for any kind of structure, we have to find an ideal number. This point is called **resolution** in programmer language.

In Figure 2.3 PML means perfectly matched layer (Berenger 1994). It absorbs EM waves at simulation boundaries without reflections. It provide us studying small

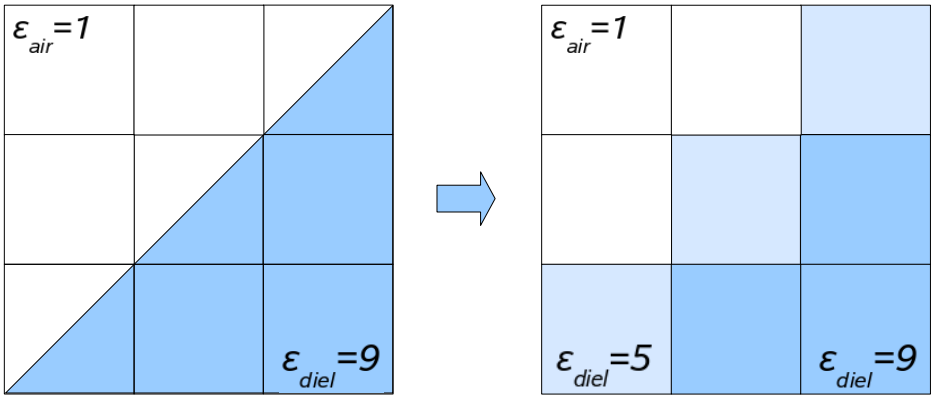

Figure 2.2. A triangular object in a Yee lattice in 2D.

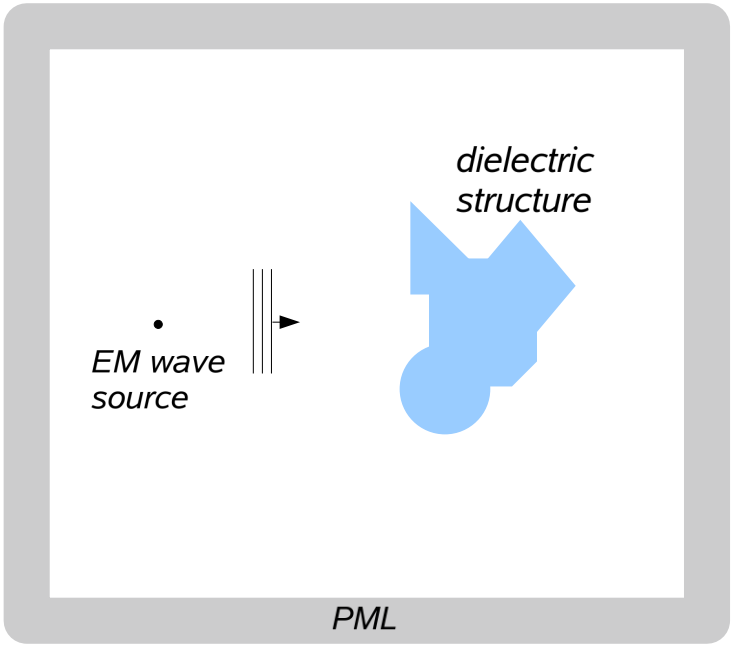

Figure 2.3. FDTD simulation space with PML which absorbs EM waves at simulation boundaries without reflections. Any kind of structure can be inserted in the simulation space.

simulation space without reflection effects from simulation boundaries. So we gain times during a computation.

In this thesis, we use **MEEP**[1] (MIT Electromagnetic Equation Propagation) software for FDTD simulations. MEEP is a free software package developed at MIT to model EM systems. It works on Linux OS.

2.2. Plane Wave Expansion Method

In Chapter 1 we said that most important properties of PhCs are the **photonic band gap** and **strong localization of EM waves** in disordered PhCs. Plane wave expansion (PWE) method is a useful tool for calculating electromagnetic band gaps and localized frequencies (Satpathy, et al. 1990, Ho, et al. 1990, Zhang and Satpathy 1990, Plihal and Maradudin 1991, Meade, et al. 1992, Sözüer 2009). *What is the origin of the PWE method?* We try to answer the question in this section. As we mentioned in Chapter 1, we studied a line defect waveguide based on 2D PhCs in this thesis, so our derivation will be for 2D PhCs.

Our starting point is again Maxwell's equations.

$$\nabla \cdot \mathbf{D} = \rho \tag{2.39}$$

$$\nabla \cdot \mathbf{B} = 0 \tag{2.40}$$

$$\nabla \times \mathbf{E} = -\frac{\partial \mathbf{B}}{\partial t} \tag{2.41}$$

$$\nabla \times \mathbf{H} = \mathbf{J} + \frac{\partial \mathbf{D}}{\partial t} \tag{2.42}$$

We assume that there are no charge density and current density in a 2D PhC.

[1] http://ab-initio.mit.edu/wiki/index.php/Meep

$$\nabla \cdot \mathbf{E} = 0 \tag{2.43}$$

$$\nabla \cdot \mathbf{H} = 0 \tag{2.44}$$

$$\nabla \times \mathbf{E} = -\mu\mu_0 \frac{\partial \mathbf{H}}{\partial t} \tag{2.45}$$

$$\nabla \times \mathbf{H} = \epsilon\epsilon_0 \frac{\partial \mathbf{E}}{\partial t} \tag{2.46}$$

where $\mathbf{D} = \epsilon\epsilon_0\mathbf{E}$ and $\mathbf{B} = \mu\mu_0\mathbf{H}$. With Eqs. 2.45-2.46

$$\nabla \times \eta\nabla \times \mathbf{H} + \frac{\mu}{c^2}\frac{\partial^2 \mathbf{H}}{\partial t^2} = 0 \tag{2.47}$$

where $\eta = \dfrac{1}{\epsilon}$ and $c = \dfrac{1}{\sqrt{\mu_0\epsilon_0}}$. Mathematically $\mathbf{H}(\mathbf{r}, t)$ can be written as an inverse Fourier transform in time and space

$$\mathbf{H}(\mathbf{r}, t) = \iint \mathbf{H}(\mathbf{k}', w) e^{i(\mathbf{k}'\cdot\mathbf{r} - wt)} d\mathbf{k}' dw. \tag{2.48}$$

On the other hand a plane wave of frequency w is written by

$$\mathbf{E}(\mathbf{r}, t) = \mathbf{E}_0 e^{i(\mathbf{k}\cdot\mathbf{r} - wt)} \tag{2.49}$$

So Equation2.48 can be thought a summation of plane waves with infinite numbers of different frequencies and wave vectors. This is the origin of the expression **plane wave expansion**. When Equation2.48 is used in Equation2.47, one obtains

$$\nabla \times \eta\nabla \times \mathbf{H}(\mathbf{r}, w) - \frac{w^2\mu}{c^2}\mathbf{H}(\mathbf{r}, w) = 0 \tag{2.50}$$

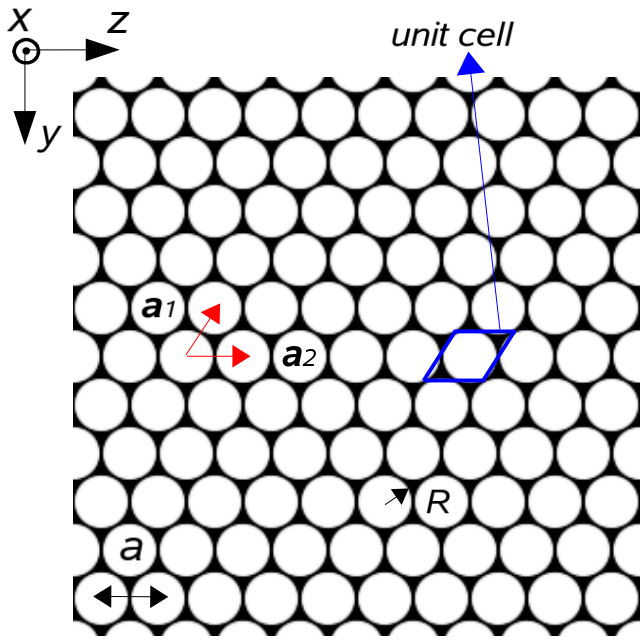

Figure 2.4. White represents air ($\epsilon_{air} = 1$), black represents dielectric material ($\epsilon_{diel} = 13$). The lattice of the PhC is triangular. So it is a 2D triangular PhC. $R = 0.48a$ is the radius of the holes. a is lattice parameter (or constant). $\mathbf{a}_1$ and $\mathbf{a}_2$ are basis vectors of the lattice. The blue parallelepiped is the unit cell of the PhC.

where

$$\mathbf{H}(\mathbf{r}, w) = \int \mathbf{H}(\mathbf{k}', w) e^{i\mathbf{k}'\cdot\mathbf{r}} d\mathbf{k}'. \tag{2.51}$$

Since our derivation is for 2D PhCs, $\mathbf{k}'$ and $\mathbf{r}$ are both in the yz plane.

In Figure 2.4, a 2D PhC is shown. White represents air, black represents dielectric material. The lattice of the PhC is triangular (or hexagonal). So the PhC is called **2D triangular PhC**. $\mathbf{a}_1$ and $\mathbf{a}_2$ are basis vectors of the lattice. The parallelepiped defined by the basis vectors is called a unit (or primitive) cell. The translation vector is in the lattice

$$\mathbf{R} = n_1\mathbf{a}_1 + n_2\mathbf{a}_2 \tag{2.52}$$

where $n_1, n_2 \in \mathbb{Z}$. Because of the periodicity

$$\eta(\mathbf{r}) = \eta(\mathbf{r}+\mathbf{R}) \quad ; \quad \mu(\mathbf{r}) = \mu(\mathbf{r}+\mathbf{R}) \tag{2.53}$$

$\eta(\mathbf{r})$ and $\mu(\mathbf{r})$ can be written as a Fourier series

$$\eta(\mathbf{r}) = \sum_{\mathbf{G}'} \eta(\mathbf{G}') e^{i\mathbf{G}'\cdot\mathbf{r}} \quad ; \quad \mu(\mathbf{r}) = \sum_{\mathbf{G}''} \mu(\mathbf{G}'') e^{i\mathbf{G}''\cdot\mathbf{r}} \tag{2.54}$$

$\mathbf{G}$ is reciprocal lattice vector given by

$$\mathbf{G} = m_1\mathbf{b}_1 + m_2\mathbf{b}_2 \quad ; \quad m_1, m_2 \in \mathbb{Z} \tag{2.55}$$

where $\mathbf{b}_1$ and $\mathbf{b}_2$ are the basis vectors of the reciprocal lattice (see Figure 2.5 for the reciprocal lattice of a triangular PhC lattice). They are given by

$$\mathbf{b}_1 = 2\pi \frac{\mathbf{a}_2 \times \hat{x}}{\mathbf{a}_1 \cdot \mathbf{a}_2 \times \hat{x}} \quad ; \quad \mathbf{b}_2 = 2\pi \frac{\hat{x} \times \mathbf{a}_1}{\mathbf{a}_1 \cdot \mathbf{a}_2 \times \hat{x}} \quad ; \quad \mathbf{a}_i \cdot \mathbf{b}_j = 2\pi\delta_{ij} \tag{2.56}$$

In addition Equation 2.51 can be written with $\mathbf{k}' \rightarrow \mathbf{k} + \mathbf{G}$

$$\mathbf{H}(\mathbf{r}, w) = \sum_{\mathbf{G}} \int_{BZ} \mathbf{H}(\mathbf{k}+\mathbf{G}, w) e^{i(\mathbf{k}+\mathbf{G})\cdot\mathbf{r}} d\mathbf{k} \tag{2.57}$$

similar to **Bloch's theorem** in solid state physics, where BZ means Brillouin zone, which is a primitive cell in the reciprocal lattice (see Figure 2.5).

When Equation 2.54-2.57 are used in Equation 2.51, we get

$$\sum_{\mathbf{G}} \eta(\mathbf{G}' - \mathbf{G})(\mathbf{k} + \mathbf{G}') \times [(\mathbf{k} + \mathbf{G}) \times \mathbf{H}(\mathbf{k} + \mathbf{G}, w)] + \frac{w^2}{c^2}\mu(\mathbf{G}' - \mathbf{G})\mathbf{H}(\mathbf{k} + \mathbf{G}, w) = 0 \quad (2.58)$$

which is a **generalized eigenvalue problem**. This method is called **H method**. The derivation of the generalized eigenvalue equation can be done in terms of electric field $\mathbf{E}$. Since Maxwell's Eqs. 2.43-2.46 are invariant under these transformation

$$\mathbf{H} \leftrightarrows \mathbf{E} \quad ; \quad \mu \leftrightarrows \epsilon \quad ; \quad \mu_0 \leftrightarrows -\epsilon_0 \quad (2.59)$$

the generalized eigenvalue equation for electric field $\mathbf{E}$ is

$$\sum_{\mathbf{G}} \zeta(\mathbf{G}' - \mathbf{G})(\mathbf{k} + \mathbf{G}') \times [(\mathbf{k} + \mathbf{G}) \times \mathbf{E}(\mathbf{k} + \mathbf{G}, w)] + \frac{w^2}{c^2}\epsilon(\mathbf{G}' - \mathbf{G})\mathbf{E}(\mathbf{k} + \mathbf{G}, w) = 0 \quad (2.60)$$

where we take $\zeta = \dfrac{1}{\mu}$. This method is called **E method**. We use E method in this thesis, since E method converges more rapidly than H method for our interested PhCs (Sözüer, et al. 1991).

2.2.1. A Comprehensible Form of the Eigenvalue Equation

The eigenvalue equation is a compact form in Equation 2.60. Then let's go on the derivation to see more clearly it. With a vector identity

$$\mathbf{A} \times (\mathbf{B} \times \mathbf{C}) = \mathbf{B}(\mathbf{A} \cdot \mathbf{C}) - \mathbf{C}(\mathbf{A} \cdot \mathbf{B}) \quad (2.61)$$

Equation 2.60 becomes

$$\sum_{\mathbf{G}} \zeta(\mathbf{G}' - \mathbf{G}) \{(\mathbf{k}+\mathbf{G}) \cdot [(\mathbf{k}+\mathbf{G}') \cdot \mathbf{E}(\mathbf{k}+\mathbf{G}, w)] - \mathbf{E}(\mathbf{k}+\mathbf{G}, w) \cdot [(\mathbf{k}+\mathbf{G}') \cdot (\mathbf{k}+\mathbf{G})]\} + \frac{w^2}{c^2}\epsilon(\mathbf{G}' - \mathbf{G})\mathbf{E}(\mathbf{k}+\mathbf{G}, w) = 0 \quad (2.62)$$

or in terms of x, y and z components of $\mathbf{E}$, $\mathbf{k}$ and $\mathbf{G}$

$$\sum_{\mathbf{G}} \zeta(\mathbf{G}' - \mathbf{G}) \{-(\mathbf{k}+\mathbf{G}) \cdot (\mathbf{k}+\mathbf{G}')E_x(\mathbf{k}+\mathbf{G}, w)\} + \frac{w^2}{c^2}\epsilon(\mathbf{G}' - \mathbf{G})E_x(\mathbf{k}+\mathbf{G}, w) = 0 \quad (2.63)$$

$$\sum_{\mathbf{G}} \zeta(\mathbf{G}' - \mathbf{G}) \{-(k'_z + G'_z)(k_z + G_z)E_y(\mathbf{k}+\mathbf{G}, w) + (k_y + G_y)(k'_z + G'_z)E_z(\mathbf{k}+\mathbf{G}, w)\} + \frac{w^2}{c^2}\epsilon(\mathbf{G}' - \mathbf{G})E_y(\mathbf{k}+\mathbf{G}, w) = 0 \quad (2.64)$$

$$\sum_{\mathbf{G}} \zeta(\mathbf{G}' - \mathbf{G}) \left\{(k'_y + G'_y)(k_z + G_z)E_y(\mathbf{k}+\mathbf{G}, w) - (k_y + G_y)(k'_y + G'_y)E_z(\mathbf{k}+\mathbf{G}, w)\right\} + \frac{w^2}{c^2}\epsilon(\mathbf{G}' - \mathbf{G})E_z(\mathbf{k}+\mathbf{G}, w) = 0 \quad (2.65)$$

Now we can see the eigenvalue equation more clearly. With

$$A_{G'G} = \zeta(\mathbf{G}' - \mathbf{G})$$

$$\begin{pmatrix} (\mathbf{k}+\mathbf{G})\cdot(\mathbf{k}+\mathbf{G}') & 0 & 0 \\ 0 & (k'_z+G'_z)(k_z+G_z) & -(k_y+G_y)(k'_z+G'_z) \\ 0 & -(k'_y+G'_y)(k_z+G_z) & (k_y+G_y)(k'_y+G'_y) \end{pmatrix} \tag{2.66}$$

$$B_{G'G} = \begin{pmatrix} \epsilon(\mathbf{G}'-\mathbf{G}) & 0 & 0 \\ 0 & \epsilon(\mathbf{G}'-\mathbf{G}) & 0 \\ 0 & 0 & \epsilon(\mathbf{G}'-\mathbf{G}) \end{pmatrix} \tag{2.67}$$

and

$$x_G = \begin{pmatrix} E_x(\mathbf{k}+\mathbf{G},w) \\ E_y(\mathbf{k}+\mathbf{G},w) \\ E_z(\mathbf{k}+\mathbf{G},w) \end{pmatrix} \quad ; \quad \lambda = \frac{w^2}{c^2} \tag{2.68}$$

Eqs. 2.63-2.65 can be written

$$\sum_{\mathbf{G}} A_{G'G}x_G - \lambda B_{G'G}x_G = 0 \tag{2.69}$$

$$\mathbf{A}\mathbf{x} = \lambda\mathbf{B}\mathbf{x} \tag{2.70}$$

This is a generalized eigenvalue equation.

G in the summation means the numbers of the points in the reciprocal lattice. Additionally **G** controls the dimension of the matrices **A** and **B** in Equation 2.70. Or it can be thought from Equation 2.57 that **G** is the number of the plane waves. Actually the numbers of the points in the reciprocal lattice is infinite, however in favor of computing this eigenvalue equation with computers, we have to take it finite. An enormous number means impossible calculation because of computer technology limits. A small number means doubtful results due to convergence problem (Sözüer, et al. 1991). So before a computation, we have to take a finite optimum number N for **G**.

2.2.2. TE and TM Modes

How can we make a decision for which EM wave is TE or TM in a 2D system? According to Poynting's theorem

$$\mathbf{S} = \frac{1}{\mu_0}(\mathbf{E} \times \mathbf{B}) \tag{2.71}$$

there are two posibility for that EM waves propagate in yz plane. One of them is

$$E_x \neq 0 \quad ; \quad E_y = E_z = 0 \tag{2.72}$$

$$H_x = 0 \quad ; \quad H_y \neq 0 \quad ; \quad H_z \neq 0 \tag{2.73}$$

This is TE mode, due to that **E** is perpendicular to propagation direction of EM wave. The other one is

$$E_x = 0 \quad ; \quad E_y \neq 0 \quad ; \quad E_z \neq 0 \tag{2.74}$$

$$H_x \neq 0 \quad ; \quad H_y = H_z = 0 \tag{2.75}$$

This is TM mode, since **H** is perpendicular to propagation direction of EM wave.

Now let's look at Equation2.70. The eigenvalue equation is block diagonal. So it can be written two independent eigenvalue equations. With

$$A'_{G'G} = \zeta(\mathbf{G}' - \mathbf{G})(\mathbf{k} + \mathbf{G}) \cdot (\mathbf{k} + \mathbf{G}') \tag{2.76}$$

$$B'_{G'G} = \epsilon(\mathbf{G}' - \mathbf{G}) \tag{2.77}$$

$$x'_G = E_x(\mathbf{k} + \mathbf{G}, w) \quad ; \quad \lambda = \frac{w^2}{c^2} \tag{2.78}$$

one of them is

$$\mathbf{A}'\mathbf{x}' = \lambda\mathbf{B}'\mathbf{x}' \tag{2.79}$$

where $E_y = E_z = 0$. Consequently Equation 2.79 is $N \times N$ generalized eigenvalue problem for TE modes according to Equation 2.73, where N is the numbers of $\mathbf{G}$.

With

$$A''_{G'G} = \zeta(\mathbf{G}' - \mathbf{G}) \begin{pmatrix} (k'_z + G'_z)(k_z + G_z) & -(k_y + G_y)(k'_z + G'_z) \\ -(k'_y + G'_y)(k_z + G_z) & (k_y + G_y)(k'_y + G'_y) \end{pmatrix} \tag{2.80}$$

$$B''_{G'G} = \begin{pmatrix} \epsilon(\mathbf{G}' - \mathbf{G}) & 0 \\ 0 & \epsilon(\mathbf{G}' - \mathbf{G}) \end{pmatrix} \tag{2.81}$$

$$x''_G = \begin{pmatrix} E_y(\mathbf{k} + \mathbf{G}, w) \\ E_z(\mathbf{k} + \mathbf{G}, w) \end{pmatrix} \quad ; \quad \lambda = \frac{w^2}{c^2}, \tag{2.82}$$

the other eigenvalue equation is

$$\mathbf{A}''\mathbf{x}'' = \lambda\mathbf{B}''\mathbf{x}'' \tag{2.83}$$

where $E_x = 0$. As a result Equation 2.83 is $2N \times 2N$ generalized eigenvalue problem for TM modes according to Equation 2.75.

2.2.3. Band Structure

What do we get from these eigenvalue equations? When we look at the generalized eigenvalue equations, it is understood that we get N frequencies, w, of TE modes (or 2N

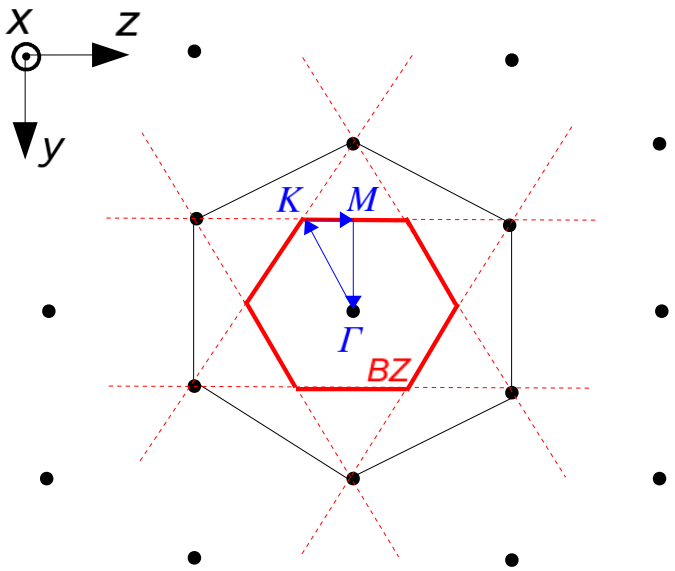

Figure 2.5. The reciprocal lattice of the triangular PhC. Brillouin zone in the reciprocal lattice. ΓKM path for values of k. w and k are dimensionless values.

frequencies, w, of TM modes) for any value of k in Brillouin zone. As the value of k is changed, we obtain a new set of N frequencies. When these frequencies are plotted for each value of k, we achieve a $w(\mathbf{k})$ function. This function is known as **band structure** or **dispersion relation**. To understand clearly this calculation, let's make an example.

2.2.3.1. An Example for Calculation of Band Structure

In a calculation of a band structure the biggest difficulty is the derivation of $\epsilon(\mathbf{G})$ for an interested PhC. According to Fourier analysis we can write

$$\epsilon(\mathbf{G}) = \frac{1}{V_{cell}} \int_{cell} \epsilon(\mathbf{r}) e^{-i(\mathbf{G}\cdot\mathbf{r})} d\mathbf{r} \tag{2.84}$$

For the 2D triangular PhC in Figure 2.4, $\epsilon(\mathbf{r})$ is

$$\epsilon(\mathbf{r}) = \epsilon_{diel} + (\epsilon_{air} - \epsilon_{diel})\Theta(R - |\mathbf{r}|) \tag{2.85}$$

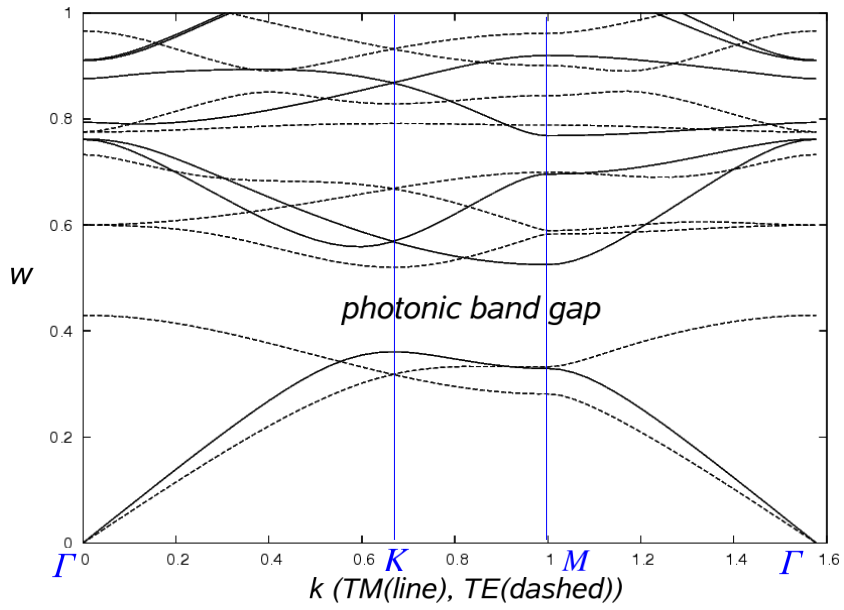

Figure 2.6. The band structure for the photonic crystal. There is a complete (TE or TM) photonic band gap between $0.42 < w < 0.53$. k values are taken on ΓKM path.

where $\Theta(x)$ is a step function and $\mathbf{r}$ is defined in unit cell. Once Equation 2.85 is used in Equation 2.84, one gets

$$\begin{aligned}
\epsilon(\mathbf{G}) &= \frac{1}{V_{cell}} \int_{cell} \epsilon_{diel} e^{-i(\mathbf{G}\cdot\mathbf{r})} d\mathbf{r} + \frac{(\epsilon_{air} - \epsilon_{diel})}{V_{cell}} \int_{cell} \Theta(R - |\mathbf{r}|) e^{-i(\mathbf{G}\cdot\mathbf{r})} d\mathbf{r} \\
&= \frac{1}{V_{cell}} \iint_{cell} \epsilon_{diel} e^{-i(G_x x + G_y y)} dx dy + \frac{(\epsilon_{air} - \epsilon_{diel})}{V_{cell}} \int_0^R \int_0^{2\pi} e^{-iGr cos\theta} d\theta r dr \\
&= \epsilon_{diel} \delta_{G_x 0} \delta_{G_y 0} + \frac{(\epsilon_{air} - \epsilon_{diel})}{V_{cell}} \int_0^R 2\pi J_0(Gr) r dr \\
&= \epsilon_{diel} \delta_{\mathbf{G}0} + (\epsilon_{air} - \epsilon_{diel}) \left(\frac{\pi R^2}{V_{cell}} \right) \frac{2J_1(GR)}{GR}
\end{aligned} \tag{2.86}$$

where $J_1(x)$ is Bessel function. So

$$\epsilon(\mathbf{G}' - \mathbf{G}) = \epsilon_{diel} \delta_{\mathbf{G}'\mathbf{G}} + (\epsilon_{air} - \epsilon_{diel}) \left(\frac{\pi R^2}{V_{cell}} \right) \frac{2J_1(|\mathbf{G}' - \mathbf{G}| R)}{|\mathbf{G}' - \mathbf{G}| R} \tag{2.87}$$

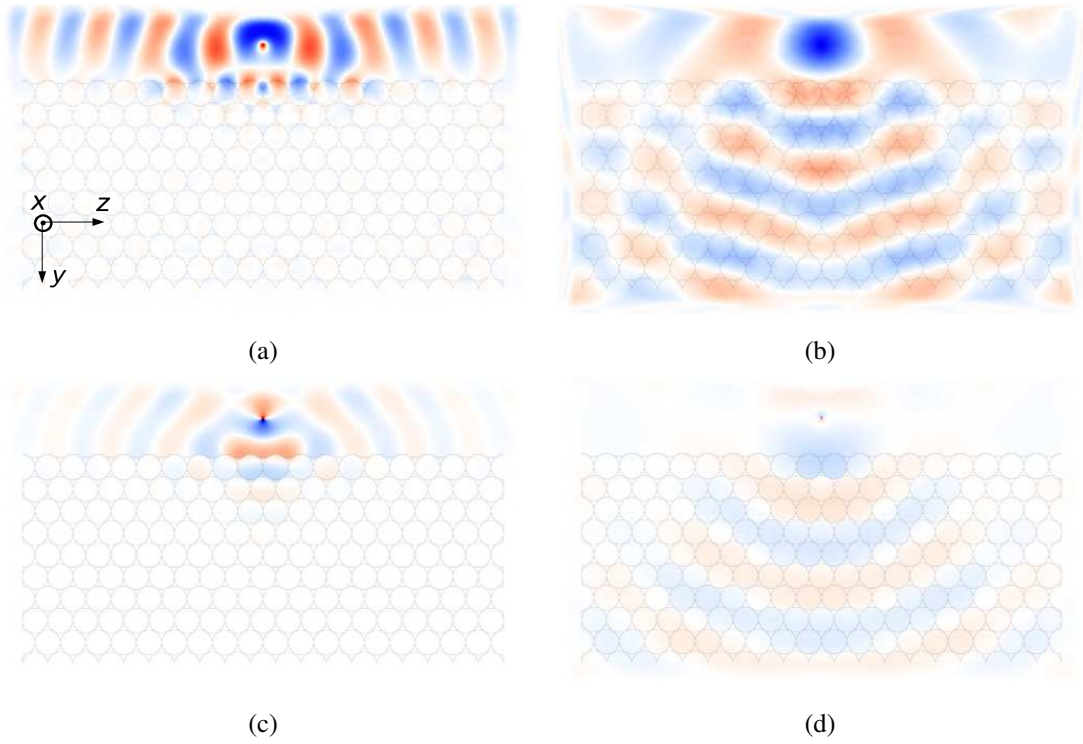

Figure 2.7. Testing the band structure with FDTD. TE modes for (a) $w = 0.45$ and (b) $w = 0.20$ frequencies. Red and blue represent the positive and negative values E_x respectively, and white regions are where the field is zero. A plot of H_x for TM modes for (c) $w = 0.45$ and (d) $w = 0.20$. The color coding is similar to that of E_x. EM waves can propagate through the PhC for $w = 0.20$. FDTD test results are consistent with the band structure.

and

$$\zeta(\mathbf{G}' - \mathbf{G}) = \zeta_{diel}\delta_{\mathbf{G}'\mathbf{G}} + (\zeta_{air} - \zeta_{diel}) \left(\frac{\pi R^2}{V_{cell}}\right) \frac{2J_1(|\mathbf{G}' - \mathbf{G}|\, R)}{|\mathbf{G}' - \mathbf{G}|\, R} \tag{2.88}$$

Because of $\mu_{air} = \mu_{diel} = 1$ or $\zeta_{air} = \zeta_{diel} = 1$, Equation 2.88 can be written

$$\zeta(\mathbf{G}' - \mathbf{G}) = \delta_{\mathbf{G}'\mathbf{G}} \tag{2.89}$$

Which values of k in Brillouin zone are used to get band structure? The reciprocal lattice for the triangular PhC structure is in Figure 2.5. ΓKM triangle repeats itself in

BZ, and it is known as the **irreducible** region of the BZ, meaning that any point in the BZ is equivalent to some point in the irreducible BZ. So it is enough to use ΓKM path for values of k. Now let's calculate the band structure of the PhC.

The calculated[2] band structure of the PhC for $R = 0.48a$ and $\epsilon_{diel} = 13$ is in Figure 2.6. The number of plane waves used in the calculation is 361. There is a complete photonic band gap between $0.42 < w < 0.53$. Compelete means that it is for TE and TM modes. w and k can be normalized so we can use the dimensionless quantities

$$\frac{wa}{2\pi c} \rightarrow w \quad ; \quad \frac{ka}{2\pi} \rightarrow k \tag{2.90}$$

The transformation is for simplicity and so the calculated band structure can be used for any value of the lattice constant a.

2.2.3.2. Testing the Band Structure with FDTD

We expect no propagation in the PhC for $w = 0.45$, which is in the complete band gap. We expect propagation in the PhC for $w = 0.20$, which is in the PhC band. *So is our prediction right?* We test the predictions for TE and TM modes in Figure 2.7 with FDTD. We use a monochromatic TE point source in Figure 2.7a-2.7b and we use a similar TM source in Figure 2.7c-2.7d. EM waves cannot propagate through the PhC in Figure 2.7a-2.7c for $w = 0.45$ frequencies and EM waves can propagate through the PhC in Figure 2.7b-2.7d for $w = 0.20$ consistent with the band structure. As a result FDTD test results are suitable with the theoretical prediction.

[2]We use FORTRAN to calculate the band structure with LAPACK (Anderson, et al. 1999) routine `dsygv`. LAPACK (Linear Algebra PACKage) is a software library for numerical linear algebra which can be obtained free of charge from `http://www.netlib.org/lapack`.

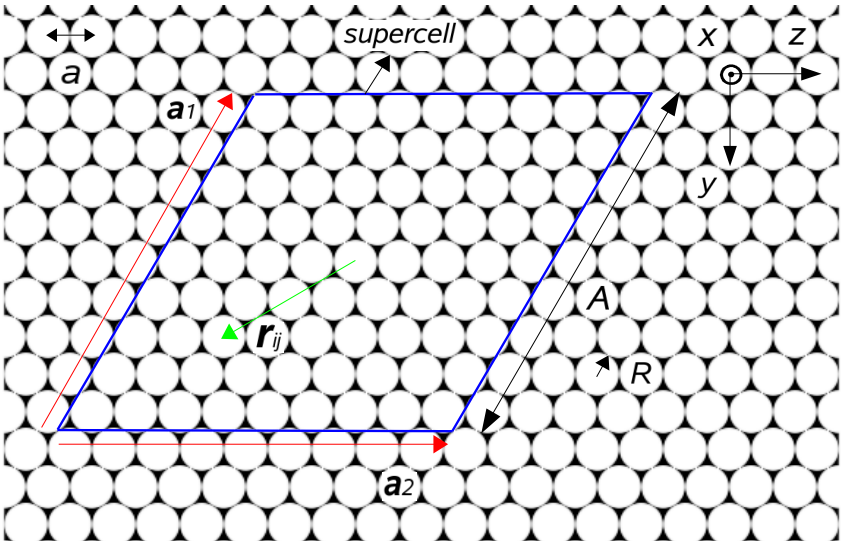

Figure 2.8. 2D triangular PhC where white represents air ($\epsilon_{air} = 1$) and black represents dielectric material ($\epsilon_{diel} = 13$). The blue parallelepiped is the chosen supercell of the PhC. $A = 9a$ is supercell size. $R = 0.48a$ is the radius of the holes. a is lattice parameter. $\mathbf{a}_1$ and $\mathbf{a}_2$ are basis vectors of the lattice. $\mathbf{r}_{ij}$ is the displacement of the holes.

2.3. Supercell Method

Supercell method is actually a plane wave expansion (PWE) method. *What is the difference then?* While a periodic part of a PhC is a unit cell in PWE method, the periodic part is chosen bigger than a unit cell in supercell method. This new periodic part instead of a unit cell is known as **supercell** and this new method is called **supercell method** (Meade, et al. 1991, Meade, et al. 1993, Sözüer 2009).

There is a 2D triangular PhC in Figure 2.8. In a calculation of a band structure with supercell method the first difficulty is again the derivation of $\epsilon(\mathbf{G})$ for an interested PhC similar to PWE method. $\epsilon(\mathbf{r})$ is for the PhC

$$\epsilon(\mathbf{r}) = \epsilon_{diel} + (\epsilon_{air} - \epsilon_{diel}) \sum_{i,j} \Theta(R - |\mathbf{r} - \mathbf{r}_{ij}|) \tag{2.91}$$

where $\Theta(x)$ is a step function and $\mathbf{r}$ is defined in supercell (SC). So we obtain

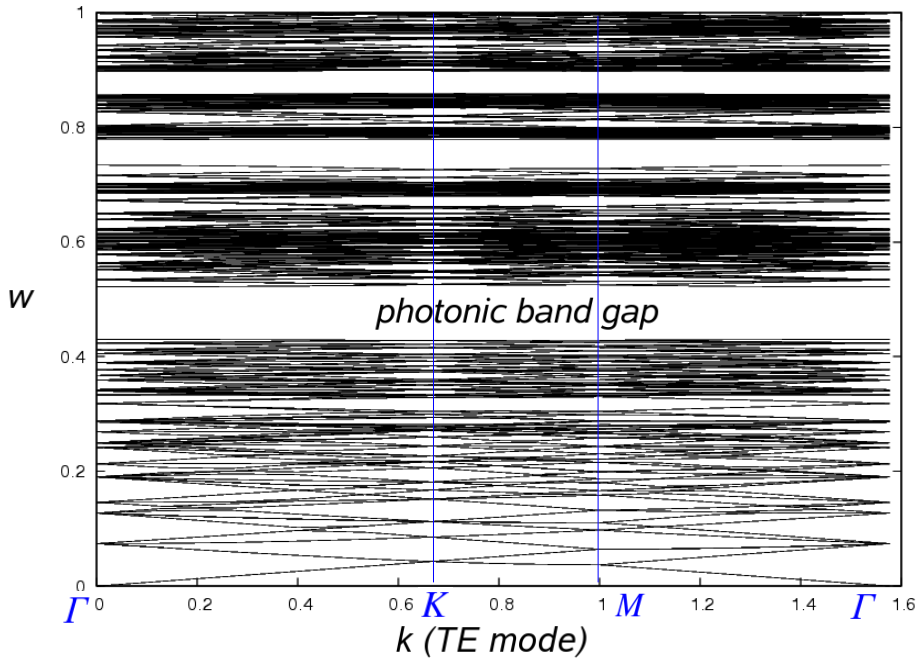

(a)

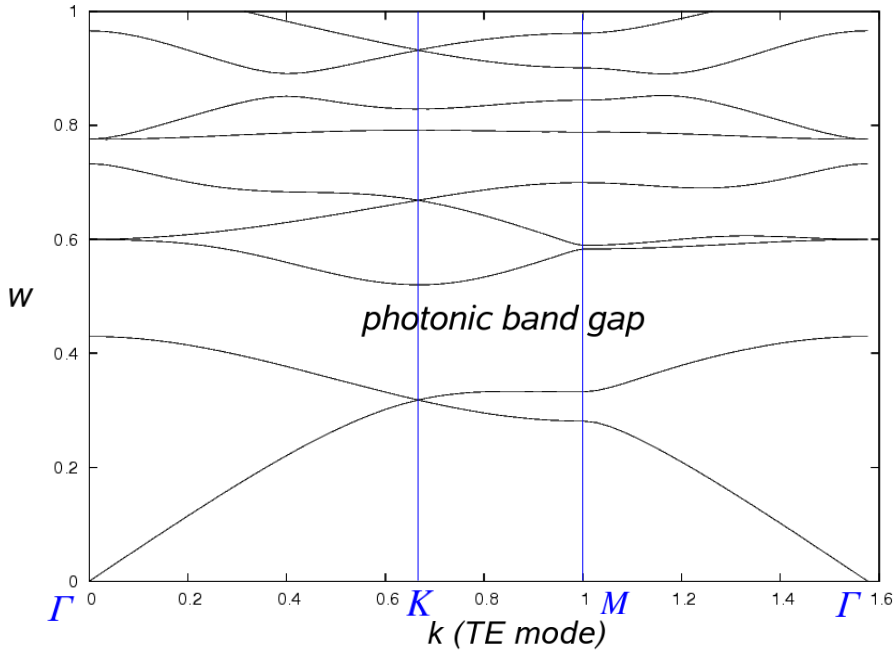

(b)

Figure 2.9. The band structure of TE modes for the PhC with (a) supercell and (b) plane wave expansion method. We achieve same photonic band gap, which is between $0.43 < w < 0.52$, with the two method.

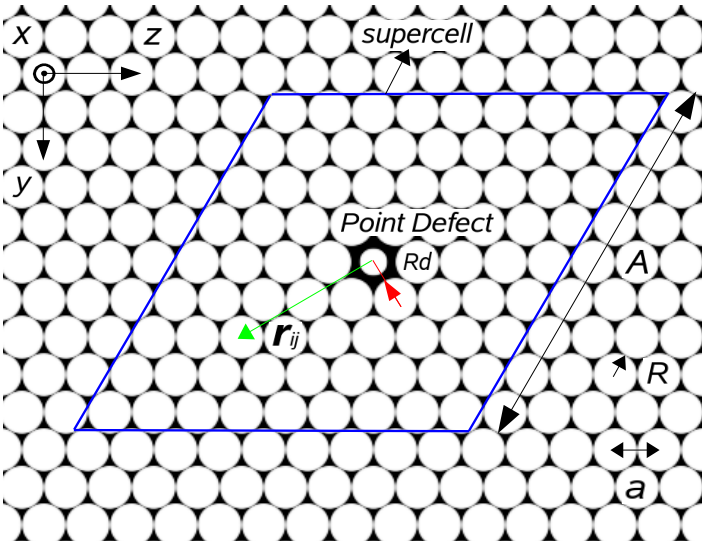

Figure 2.10. A 2D triangular PhC with point defect where white represents air ($\epsilon_{air} = 1$) and black represents dielectric material ($\epsilon_{diel} = 13$). The blue parallelepiped is the chosen supercell of the PhC. $A = 9a$ is supercell size. $R = 0.48a$ is the radius of the holes. $R_d = 0.30a$ is the radius of the point defect hole. a is lattice parameter. $\mathbf{r}_{ij}$ is the displacement of the holes.

$$\begin{aligned}\epsilon(\mathbf{G}) &= \frac{1}{V_{SC}} \int_{SC} \epsilon(\mathbf{r}) e^{-i(\mathbf{G}\cdot\mathbf{r})} d\mathbf{r} \\ &= \epsilon_{diel}\delta_{\mathbf{G}0} + (\epsilon_{air} - \epsilon_{diel}) \sum_{i,j} \cos(\mathbf{G}\cdot\mathbf{r}_{ij}) (\frac{\pi R^2}{V_{SC}}) \frac{2J_1(GR)}{GR}\end{aligned} \tag{2.92}$$

where $J_1(x)$ is Bessel function.

By using generalized eigenvalue equation for TE modes (see Equation 2.79), the band structure of the PhC for $R = 0.48a$ and $\epsilon_{diel} = 13$ with supercell method is in Figure 2.9a. Supecell size $A = 9a$. We use 8281 plane waves. There is a photonic band gap between $0.43 < w < 0.52$. w and k in the band structure are dimensionless with these transformation

$$\frac{wa}{2\pi c} \rightarrow w \quad ; \quad \frac{kA}{2\pi} \rightarrow k \tag{2.93}$$

In Figure 2.9b, same structure is calculated with PWE method by using generalized eigenvalue equation for TE modes (see Equation 2.79). We use 361 plane waves.

And we achieve same photonic band gap, which is between $0.43 < w < 0.52$. When we compare two method, we can think that PWE method is more easy than supercell method, since we use 361 plane waves instead of 8281 plane waves. *Then why do we use supercell method?*

There is a 2D hexagonal PhC with point defect in Figure 2.10. $\epsilon(\mathbf{G})$ can be easily seen from Equation 2.92 for the PhC with point defect

$$\epsilon(\mathbf{G}) = \epsilon_{diel}\delta_{\mathbf{G}0} + (\epsilon_{air} - \epsilon_{diel})(\frac{\pi R_d^2}{V_{SC}})\frac{2J_1(GR_d)}{GR_d} + (\epsilon_{air} - \epsilon_{diel})\sum_{i,j\neq 0}\cos(\mathbf{G}\cdot\mathbf{r}_{ij})(\frac{\pi R^2}{V_{SC}})\frac{2J_1(GR)}{GR} \quad (2.94)$$

By using Equation 2.79 the band structure of the PhC with point defect for $R = 0.48a$, $R_d = 0.30a$ and $\epsilon_{diel} = 13$ with supercell method is in Figure 2.11a. The band structure is for TE modes. Supecell size $A = 9a$. And we use 8281 plane waves. There is a **defect frequency** near $w = 0.46$. Now let's calculate E_x from Equation 2.79 for a band defect frequency $w = 0.4643$. Equation 2.51 can be written for electric field

$$\mathbf{E}(\mathbf{r}, w) = \sum_{\mathbf{G}}\int_{BZ}\mathbf{E}(\mathbf{k}+\mathbf{G}, w)e^{i(\mathbf{k}+\mathbf{G})\cdot\mathbf{r}}d\mathbf{k} \quad (2.95)$$

$$= \int_{BZ}\left[\sum_{\mathbf{G}}\mathbf{E}(\mathbf{k}+\mathbf{G}, w)e^{i\mathbf{G}\cdot\mathbf{r}}\right]e^{i\mathbf{k}\cdot\mathbf{r}}d\mathbf{k} \quad (2.96)$$

$$= \int_{BZ}\mathbf{E}(\mathbf{k}, \mathbf{r}, w)e^{i\mathbf{k}\cdot\mathbf{r}}d\mathbf{k} \quad (2.97)$$

where

$$\mathbf{E}(\mathbf{k}, \mathbf{r}, w) = \sum_{\mathbf{G}}\mathbf{E}(\mathbf{k}+\mathbf{G}, w)e^{i\mathbf{G}\cdot\mathbf{r}} \quad (2.98)$$

According to Equation 2.98, E_x component of electric field is in Figure 2.11b at defect frequency $w = 0.4643$. FDTD result is for defect frequency $w = 0.4643$ in

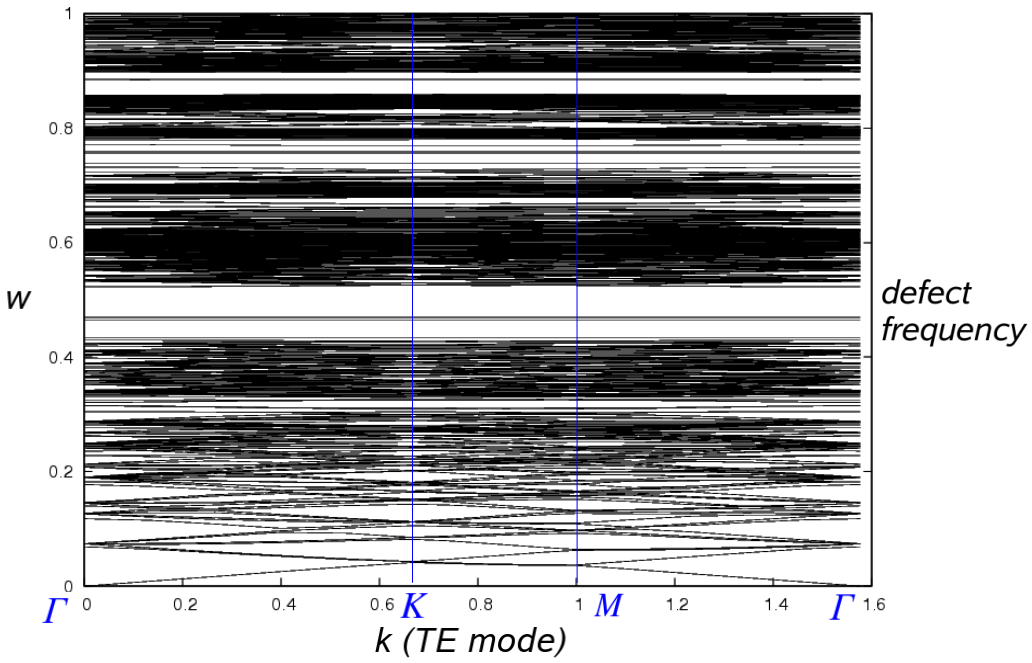

(a)

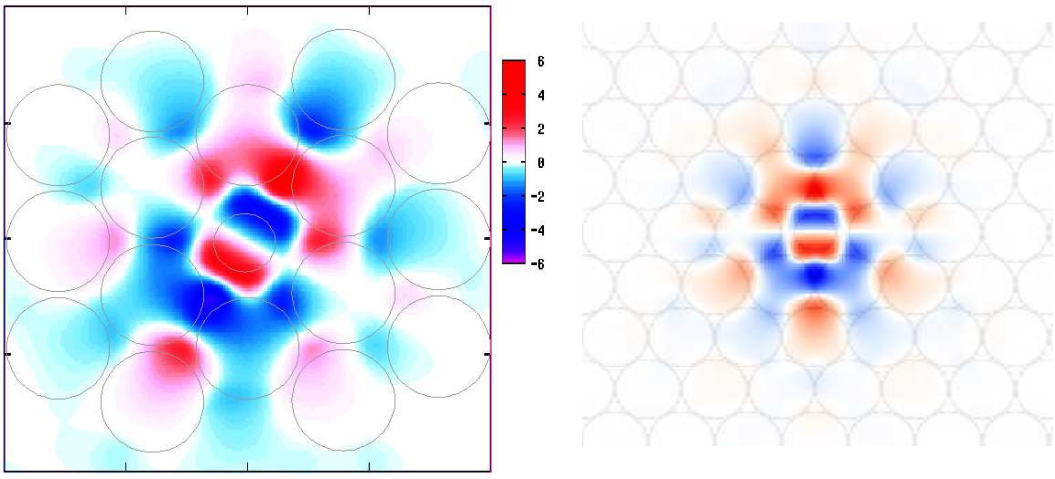

(b) (c)

Figure 2.11. (a) The band structure of TE modes for the PhC with point defect. The band structure is calculated by supercell method. (b) E_x component of electric field, which is computed by supercell method, at defect frequency $w = 0.4643$. (c) FDTD result for defect frequency $w = 0.4643$. The FDTD result is same with supercell method.

Figure 2.11c. The FDTD result is same with supercell method. It is understood that supercell method is used for computing band structures of certain disordered PhCs.

On the other hand **strongly localized EM waves** has been achieved in the disorder (the point defect for this example), which is one the most important properties of PhCs as we mentioned in Chapter 1.

CHAPTER 3

THE FREQUENCY SPLITTING DEVICE

As we mentioned briefly in Section 1.3, our frequency splitting device, or demultiplexer, is used for separating signals with different frequencies. *How does it work?* We will answer the question in this chapter.

We will build our demultiplexer using a 2D triangular PhC, shown in Figure 3.1. The band structure of the PhC is shown in Figure 3.2. The band structre is calculated by PWE method for TE modes. There is a band gap between $0.410 < w < 0.456$.

To make a frequency splitting device out of this PhC, we will use two different line defect PhC waveguides, each supporting propagation at a different frequency. The line defect is formed by changing the radii of a line of air holes. As mentioned in Section 2.3, we use the supercell method for calculating the band structure of the PhCs with line defects. The supercell is shown in Figure 3.3a, and the band structure of the PhC with supercell method for TE modes is in Figure 3.3b. For purposes of comparison, we first take $R_d = R = 0.455a$ to obtain the waveguide dispersion for the perfect superlattice, with $A = 30\sqrt{3}a$. There is a band gap between $0.410 < w < 0.456$, which is same with the band structure calculated by PWE method. Now let's calculate the band structure of the PhC waveguides with actual line defects, i.e. with $R_d \neq R$, to observe the differences between the two cases.

3.1. The Photonic Crystal Waveguide with the Line Defect-1

In Figure 3.4a, there is the PhC waveguide with line defect-1 where the radius of the holes on the line defect is $R_d = 0.423a$. The band structure for the PhC waveguide is in Figure 3.4b. The **defect band** (or **guided mode**) is in $0.433 < w < 0.456$. For $0.442 < w < 0.456$, there are single guided modes. For $0.433 < w < 0.442$, there are double guided modes whose grup velocities are different ($v_g = \frac{dw}{dk}$).

E_z component of electric field, which is calculated by supercell method, is for

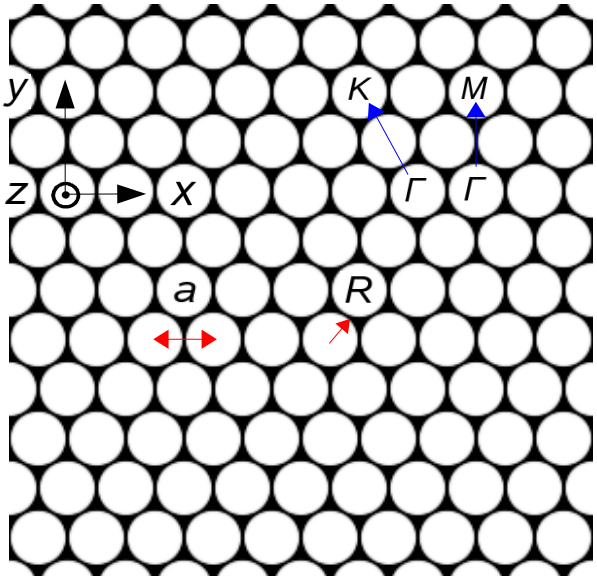

Figure 3.1. A 2D hexagonal PhC where black and white represent $\epsilon_{diel} = 11.7$ and $\epsilon_{air} = 1$ respectively. The hole radius is $R = 0.455a$. a is lattice parameter. Blue arrows represent ΓK and ΓM directions

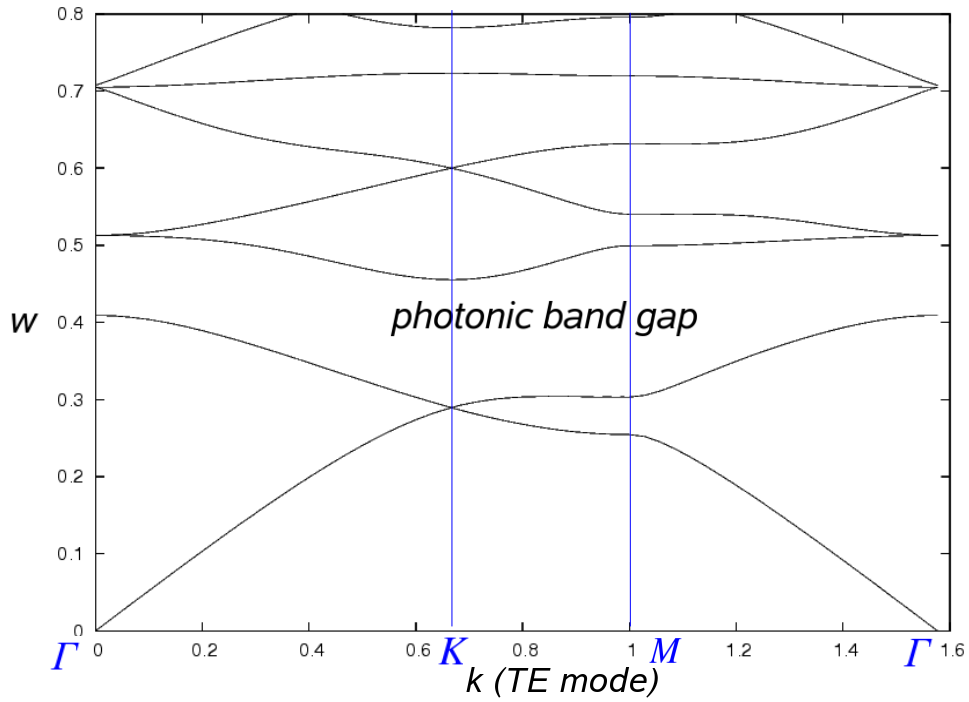

Figure 3.2. The band structure of the perfect PhC with PWE method for TE modes. There is a band gap between $0.410 < w < 0.456$. w and k are dimensionless values.

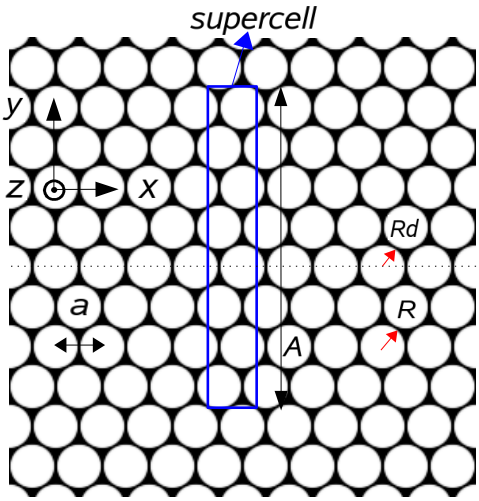

(a)

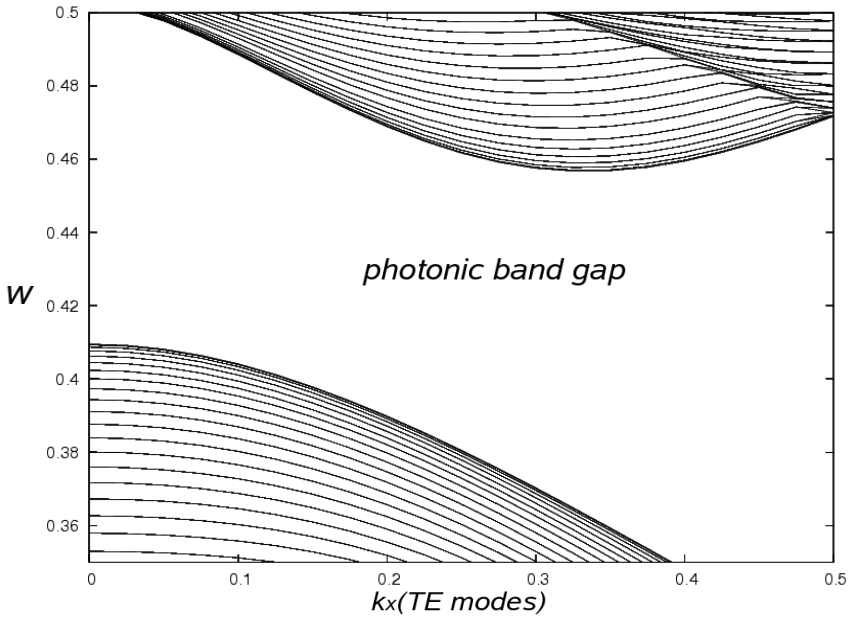

(b)

Figure 3.3. (a) A 2D triangular PhC where white represents air ($\epsilon_{air} = 1$) and black represents dielectric material ($\epsilon_{diel} = 11.7$). The blue rectangle is the chosen supercell of the PhC. The supercell size is $a \times A$, where A is roughly $8a$ in the graph, although in the actual calculations, we used a much larger value, $A = 30\sqrt{3}a$. For a perfect lattice with no line defects, $R_d = R = 0.455a$ is the radius of the holes, and a is the lattice constant. (b) The band structure of the perfect PhC for TE modes with supercell method. There is a band gap between $0.410 < w < 0.456$, which is same at the band structure calculated by PWE method.

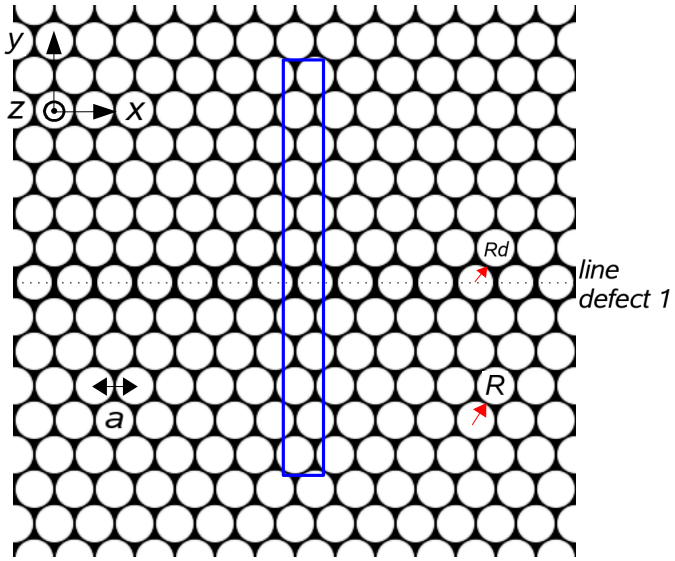

(a)

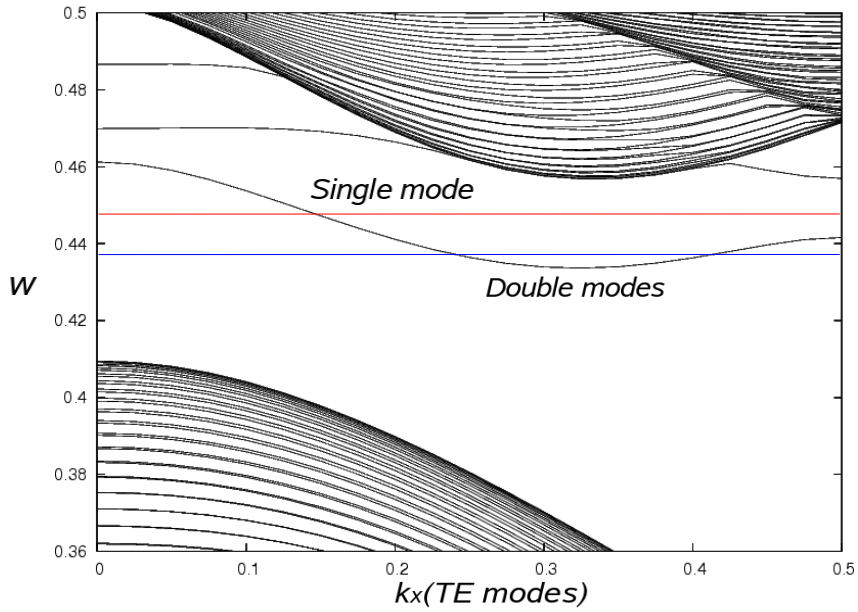

(b)

Figure 3.4. (a) The PhC waveguide with line defect-1 where white represents air ($\epsilon_{air} = 1$) and black represents dielectric material ($\epsilon_{diel} = 11.7$). The blue rectangle is the chosen supercell of the PhC. $R = 0.455a$ is the radius of the holes. $R_d = 0.423a$ is the radius of the holes on the line defect. a is lattice parameter. (b) The band structure of the PhC waveguide with line defect-1 for TE modes with supercell method. The defect band is in $0.433 < w < 0.456$. For $0.442 < w < 0.456$, there is a single guided mode. For $0.433 < w < 0.442$, there are double guided modes whose grup velocities are different.

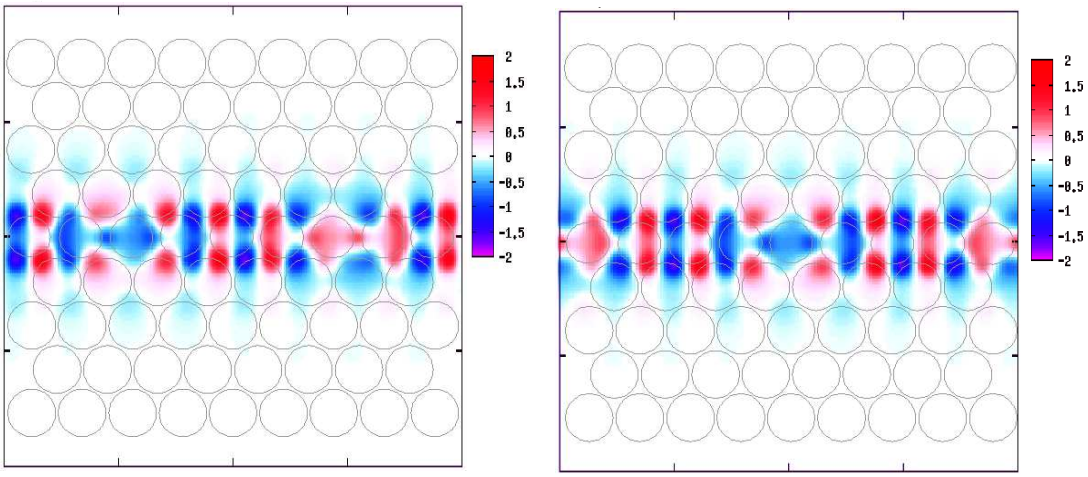

(a) Odd function

(b) Even function

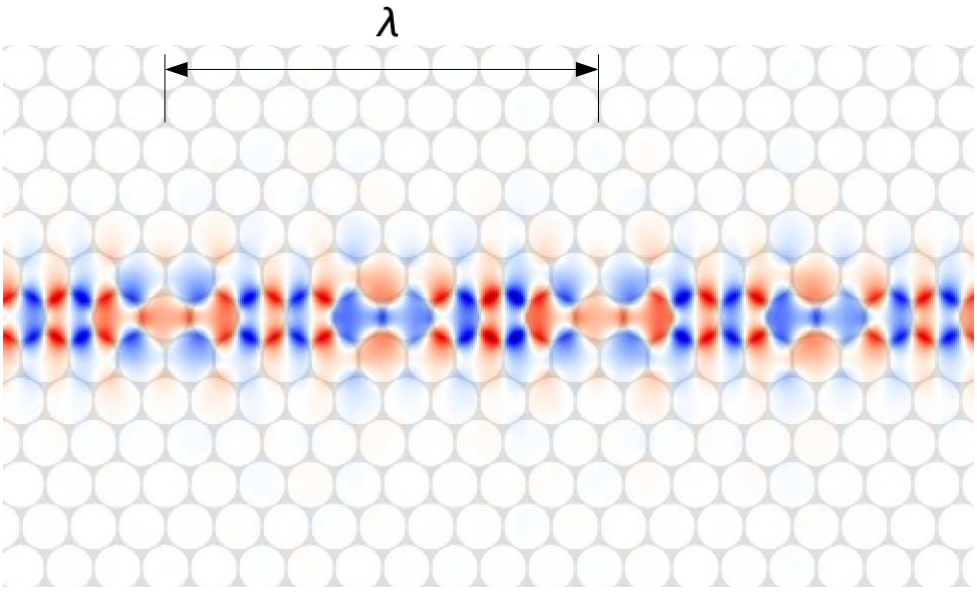

(c)

Figure 3.5. (a) and (b) E_z component of electric field, which is calculated by super-cell method, is for a guided mode frequency $w = 0.450$ for the PhC waveguide with line defect-1. (c) FDTD simulation for a guided mode frequency $w = 0.450$. Red and blue represent the positive and negative values E_z respectively, and white regions are where the field is zero. The FDTD simulation is very similar to the calculated E_z. $\lambda \approx 9a$ is found from the FDTD simulation.

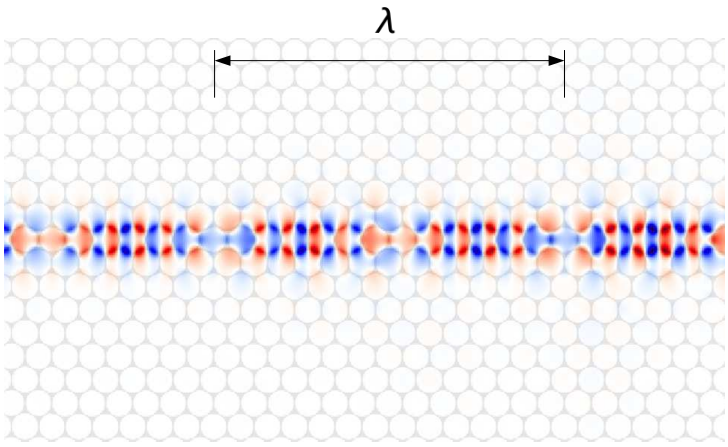

(a)

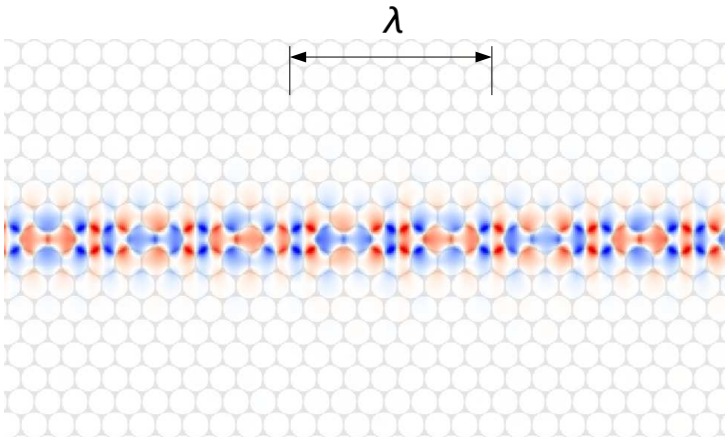

(b)

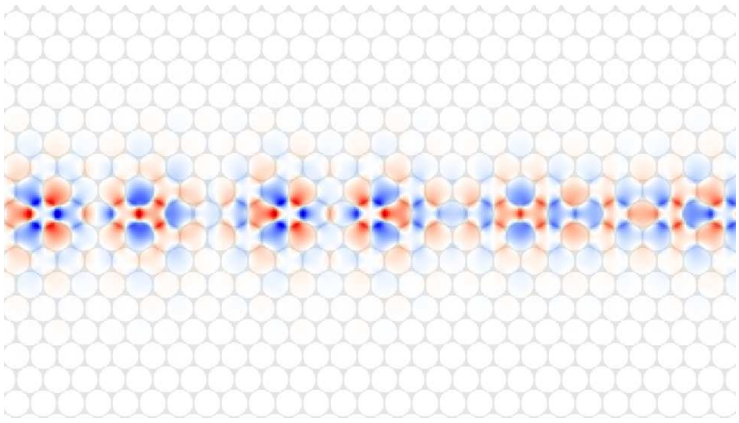

(c)

Figure 3.6. FDTD simulation at (a) $w = 0.454$, (b) $w = 0.447$,(c) $w = 0.437$ for the PhC waveguide with line defect-1. At $w = 0.454$ and $w = 0.447$ frequencies, there is a single mode guidance consistent with the band structure. For $w = 0.454$ frequency, $\lambda \approx 13a$ is found. For $w = 0.447$ frequency, $\lambda \approx 7.5a$ is found. There is a double mode guidance for $w = 0.437$ frequency. So superposition takes place and λ cannot be found.

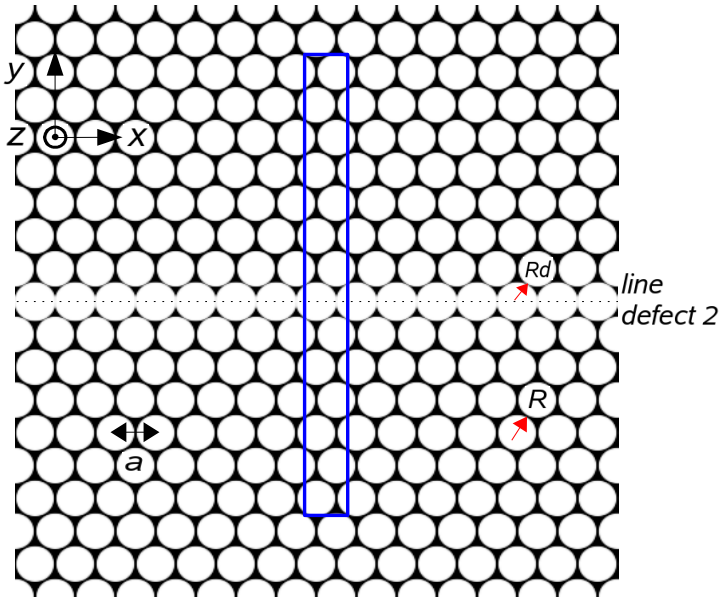

(a)

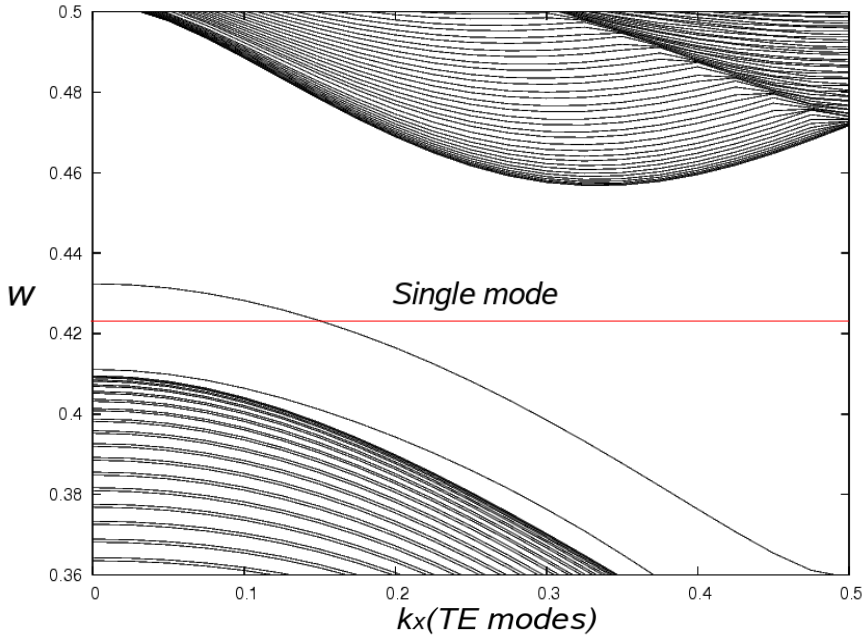

(b)

Figure 3.7. (a) The PhC waveguide with line defect-2 where white represents air ($\epsilon_{air} = 1$) and black represents dielectric material ($\epsilon_{diel} = 11.7$). The blue rectangle is the chosen supercell of the PhC. $R = 0.455a$ is the radius of the holes. $R_d = 0.500a$ is the radius of the holes on the line defect. a is lattice parameter. (b) The band structure of the PhC waveguide with line defect-2 for TE modes with supercell method. The defect band is in $0.410 < w < 0.433$. There is a single guided mode.

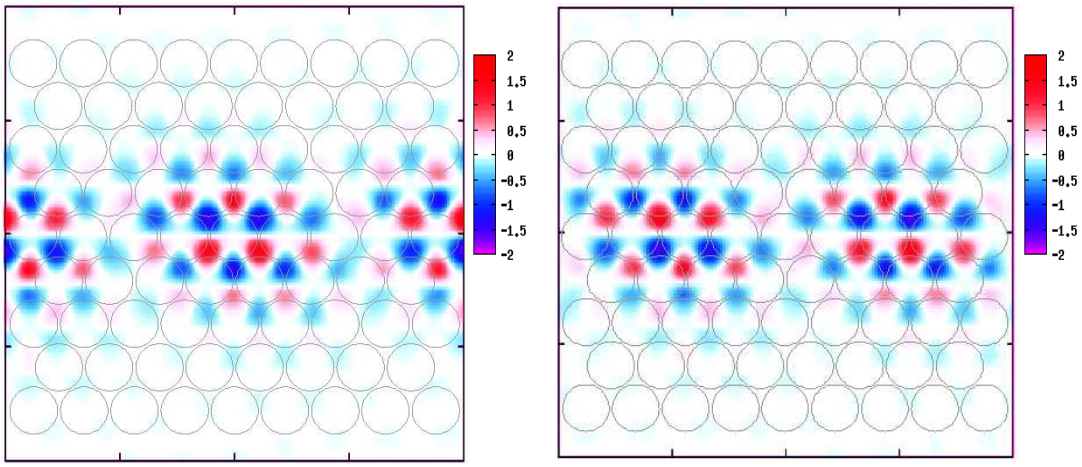

(a) Odd function

(b) Even function

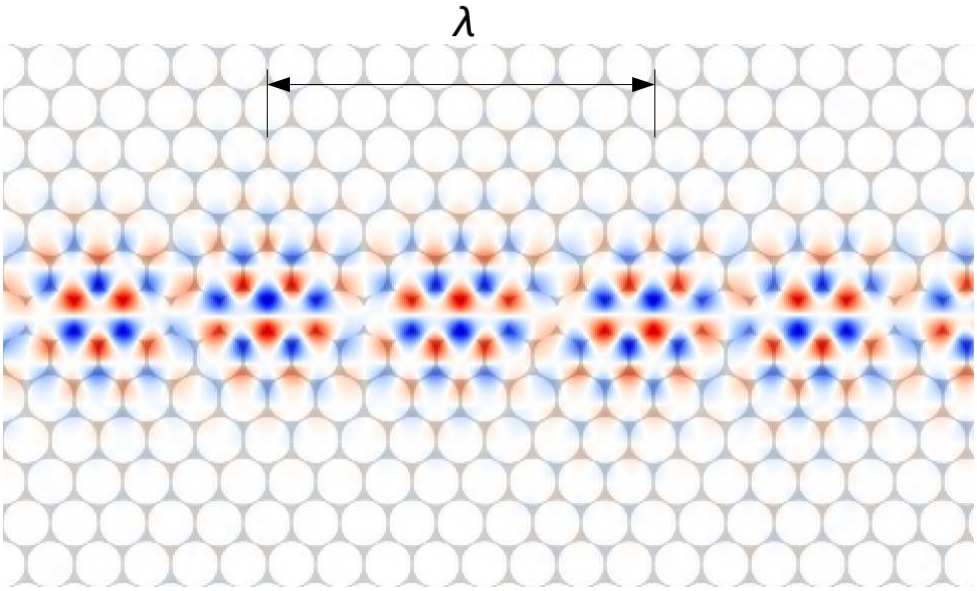

(c)

Figure 3.8. (a) and (b) E_z component of electric field, calculated by supercell method, is for a guided mode frequency $w = 0.423$ for the PhC waveguide with line defect-2. (c) FDTD simulation for a guided mode frequency $w = 0.423$. The FDTD simulation is very similar to the calculated E_z. $\lambda \approx 8a$ is found from the FDTD simulation.

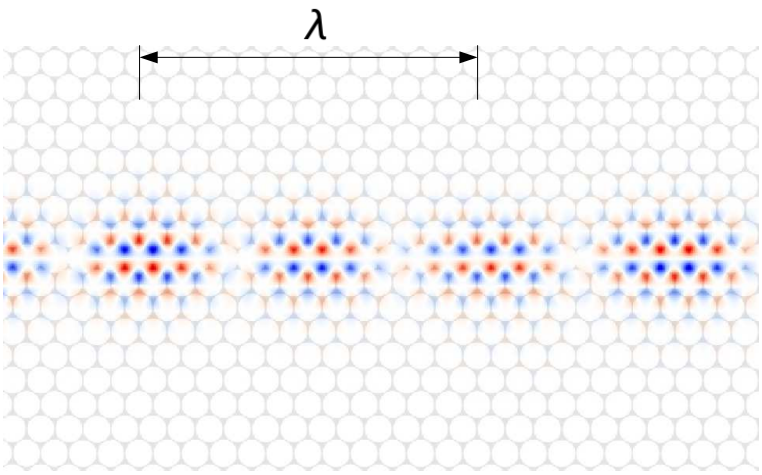

(a)

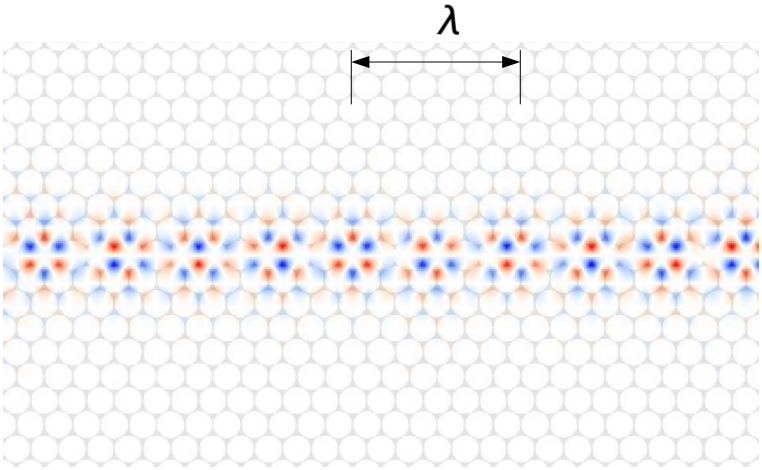

(b)

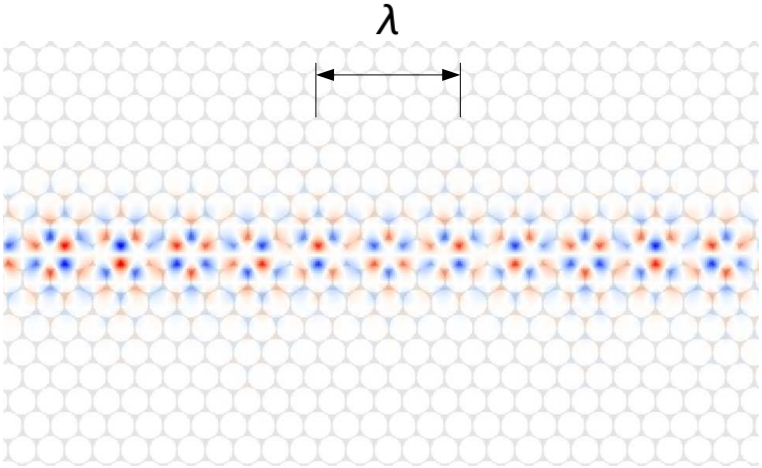

(c)

Figure 3.9. FDTD simulation at (a) $w = 0.428$, (b) $w = 0.418$,(c) $w = 0.413$ for the PhC waveguide with line defect-2. At all frequencies, there is a single mode guidance consistent with the band structure. For $w = 0.428$, $w = 0.418$ and $w = 0.413$ frequencies, $\lambda \approx 12a$, $\lambda \approx 6a$ and $\lambda \approx 5a$ are found respectively.

a guided mode frequency $w = 0.450$ in Figure 3.5a-3.5b for the PhC waveguide. In Figure 3.5c, there is a FDTD simulation result for the guided mode frequency $w = 0.450$. The simulation picture is very similar to the calculated one in Figure 3.5a-3.5b. EM wave is guided in the line defect. $\lambda \approx 9a$ is found from the FDTD simulation. According to Figure 3.4b, $\lambda \lesssim 10a$ for $w = 0.450$ frequency [1]. λ can be calculated with two different way.

FDTD simulations are for $w = 0.454$ and $w = 0.447$ in Figure 3.6a-3.6b. At $w = 0.454$ and $w = 0.447$ frequencies, there is a single mode guidance. For $w = 0.454$ frequency, $\lambda \approx 13a$ is found. For $w = 0.447$ frequency, $\lambda \approx 7.5a$ is found. The values of λ are appropriate with the band structure.

FDTD simulation is for $w = 0.437$ in Figure 3.6c. There is a double mode guidance for $w = 0.437$ frequency. So superposition takes place in Figure 3.6c. And λ cannot be found. Double mode guidance is a problem for long length PhC waveguide, because of different group velocities. However as we will see later, our PhC demultiplexer is made of short length PhC waveguides. So the problem is not important very much for us.

3.2. The Photonic Crystal Waveguide with the Line Defect 2

In Figure 3.7a, there is the PhC waveguide with line defect-2 where the radius of the holes on the line defect is $R_d = 0.500a$. The band structure for the PhC waveguide is in Figure 3.7b. There is single guided modes between $0.410 < w < 0.433$.

E_z component of electric field, which is calculated by supercell method, is for a guided mode frequency $w = 0.423$ in Figure 3.8a-3.8b for the PhC waveguide. In Figure 3.8c, there is a FDTD simulation result for the guided mode frequency $w = 0.423$. The simulation picture is very similar to the calculated one. EM wave is guided in the line defect. $\lambda \approx 8a$ is found from the FDTD simulation. According to Figure 3.7b, $\lambda \gtrsim 5a$ for $w = 0.423$ frequency [2]. λ can be calculated with two different way.

FDTD simulations are for $w = 0.428$, $w = 0.418$ and $w = 0.413$ in Figure 3.9. At all frequencies, there is a single mode guidance. For $w = 0.428$, $w = 0.418$ and

[1] Because of $\frac{ka}{2\pi} = \frac{a}{\lambda} \gtrsim 0.1$ for $w = 0.450$ frequency in Figure 3.4b, we find $\lambda \lesssim 10a$.

[2] Because of $\frac{ka}{2\pi} = \frac{a}{\lambda} \lesssim 0.2$ for $w = 0.423$ frequency in Figure 3.7b, we find $\lambda \gtrsim 5a$.

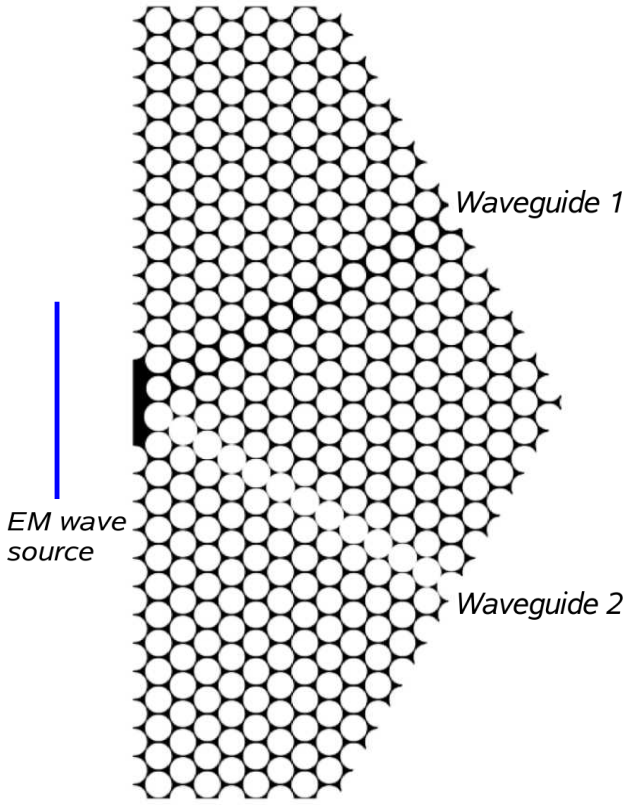

Figure 3.10. The frequency splitting device. The waveguide-1, the radius of the holes on the line defect is $R_d = 0.423a$, is at the upper half part of the device. The waveguide-2, the radius of the holes on the line defect is $R_d = 0.500a$, is at the lower half part of the device.

$w = 0.413$ frequencies, $\lambda \approx 12a$, $\lambda \approx 6a$ and $\lambda \approx 5a$ are found respectively. The values of λ are appropriate with the band structure.

3.3. The PhC Demultiplexer

Our frequency splitting device (or PhC demultiplexer) is in Figure 3.10. The waveguide-1, the radius of the holes on the line defect is $R_d = 0.423a$, is at the upper half part of the device. The waveguide-2, the radius of the holes on the line defect is $R_d = 0.500a$, is at the lower half part of the device. The testing results for guided mode frequencies ($w = 0.445$ and $w = 0.415$) are in Figure 3.11a and Figure 3.11b respectively. EM waves are guided in the PhC waveguides. The output signal is good at the end of the

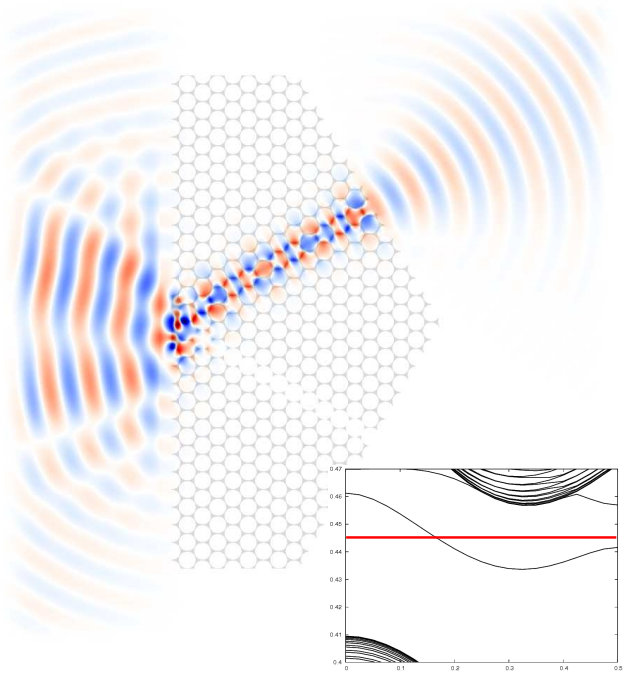

(a)

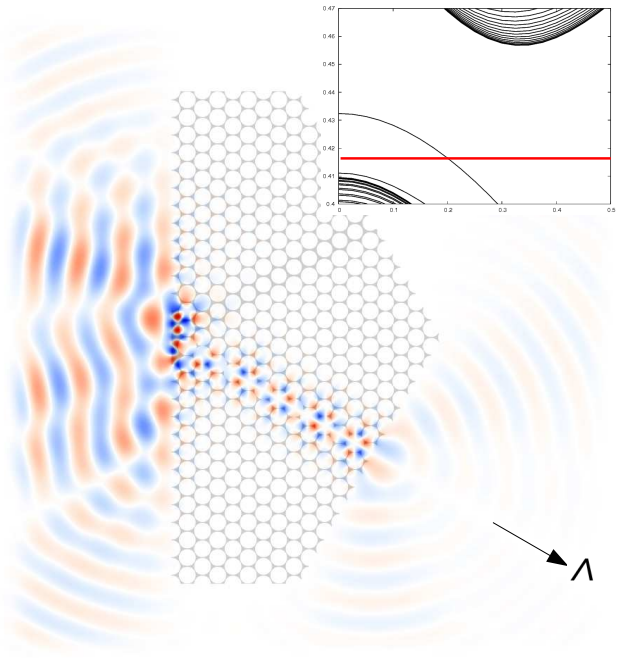

(b)

Figure 3.11. (a) The testing result for a guided mode frequency $w = 0.445$. EM waves are guided in the PhC waveguide-1. The output signal is good at the end of the PhC waveguide-1. (b) The testing result for a guided mode frequency $w = 0.415$. EM waves are guided in the PhC waveguide-2. However there is no propagation of EM waves through Λ direction at the end of the PhC waveguide-2

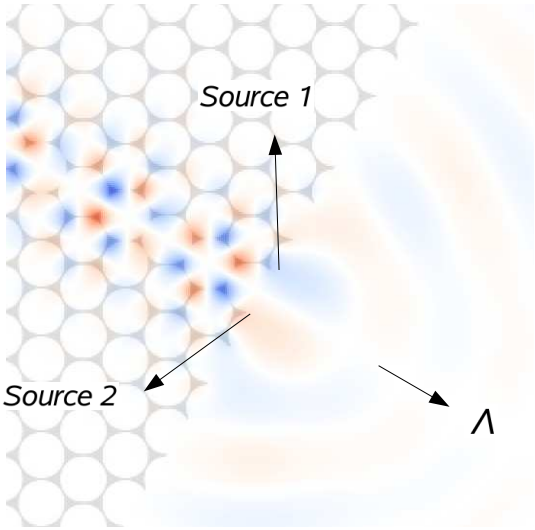

Figure 3.12. The end of the PhC waveguide-2. It can be thought two point source with a phase difference of π. There is no propagation through Λ direction because of destructive interference.

PhC waveguide-1. However there is no propagation of EM waves through Λ direction at the end of the PhC waveguide-2.

When we look at the FDTD result for $w = 0.415$ in Figure 3.12, we ask a question. *Why there isn't a propagation through* Λ *direction?* The end of the PhC waveguide-2 can be thought two point source with a phase difference of π. So two EM waves involve in destructive interference through Λ direction.

To solve the problem, let's destroy one of the two sources (see Figure 3.13). FDTD result is in Figure 3.14 for the modified end of the PhC waveguide-2 for $w = 0.415$ frequency. The output signal can go through Λ direction anymore. FDTD results are for other guided mode frequencies in the Figure 3.15-3.16-3.17-3.18.

3.4. Flux Measurement Results

As we know that Poynting's vector is

$$\mathbf{S} = \frac{1}{\mu_0}(\mathbf{E} \times \mathbf{B}) \tag{3.1}$$

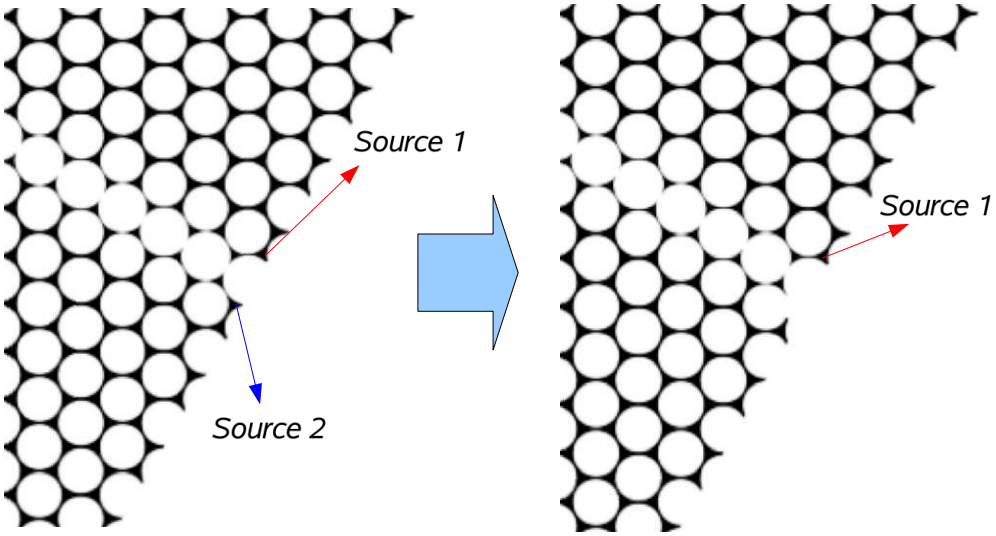

Figure 3.13. The modified end of the waveguide-2.

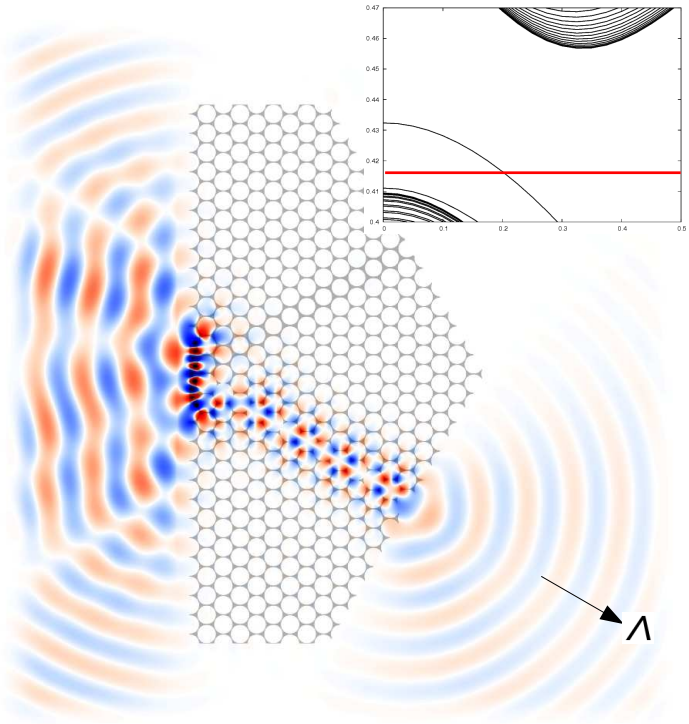

Figure 3.14. FDTD result for the modified end of the PhC waveguide-2 for $w = 0.415$ frequency. There is a propagation through Λ direction anymore.

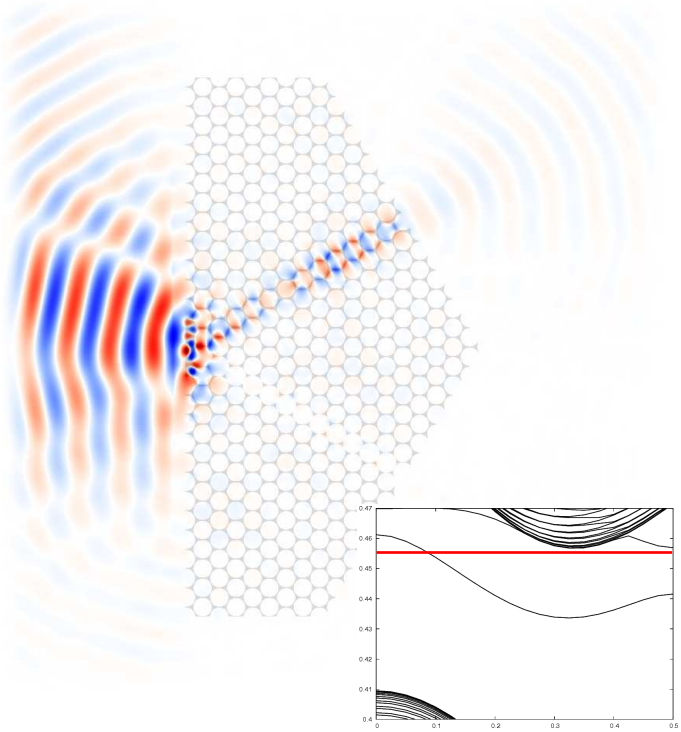

(a)

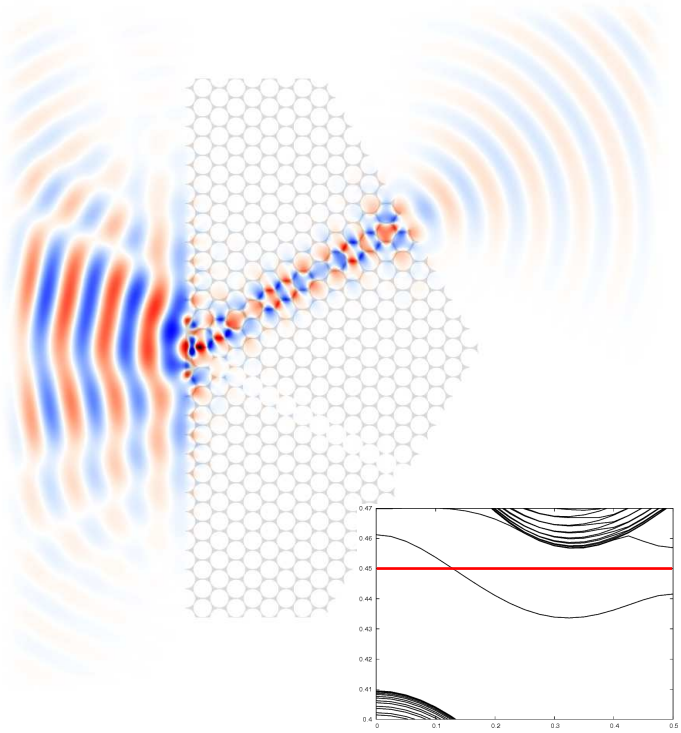

(b)

Figure 3.15. FDTD simulation for (a) $w = 0.455$, (b) $w = 0.450$. EM waves are splitted very well with the PhC waveguide-1.

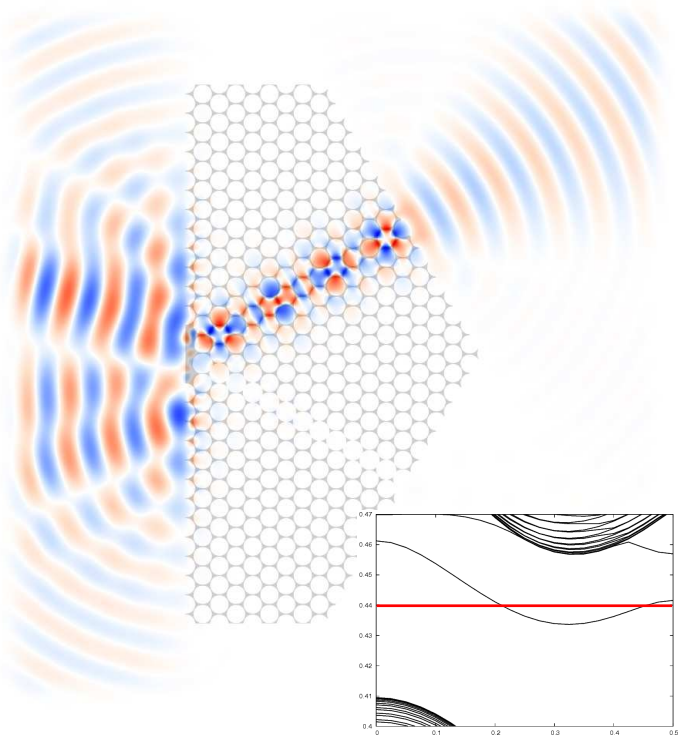

(a)

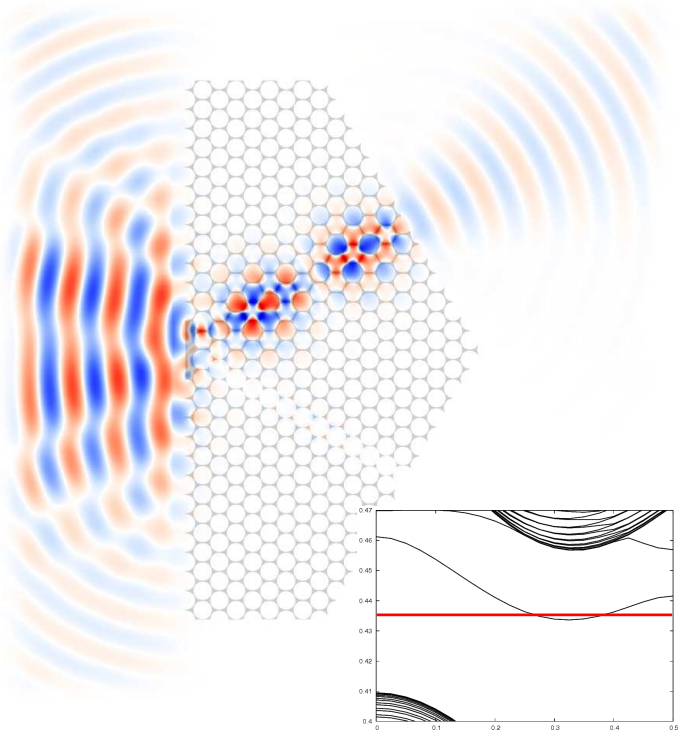

(b)

Figure 3.16. FDTD simulation for (a) $w = 0.440$ and (b) $w = 0.435$. EM waves are splitted very well with the PhC waveguide-1.

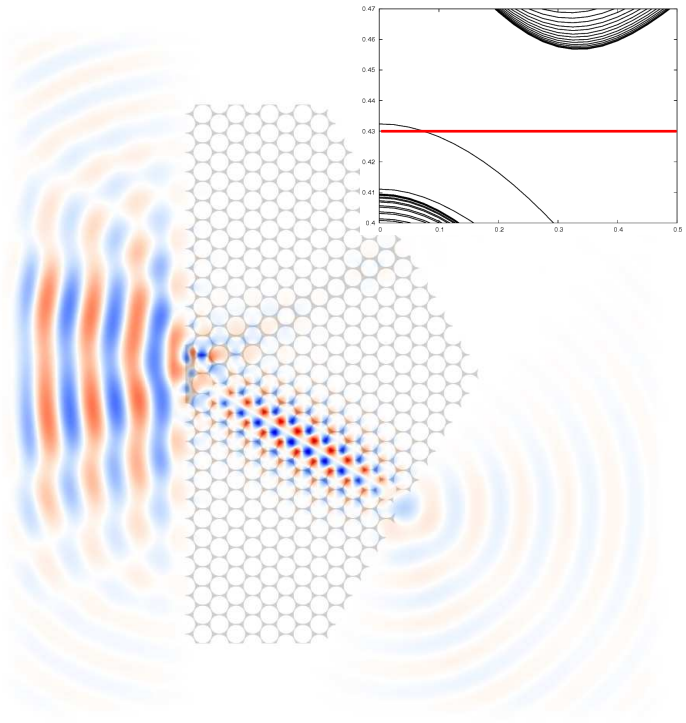

(a)

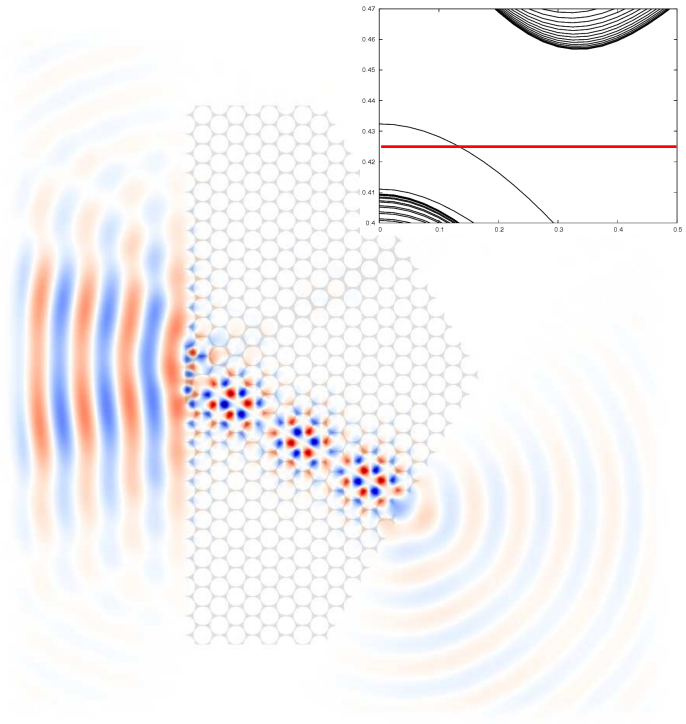

(b)

Figure 3.17. FDTD simulation for (a) $w = 0.430$, (b) $w = 0.425$. EM waves are splitted very well with the PhC waveguide-2.

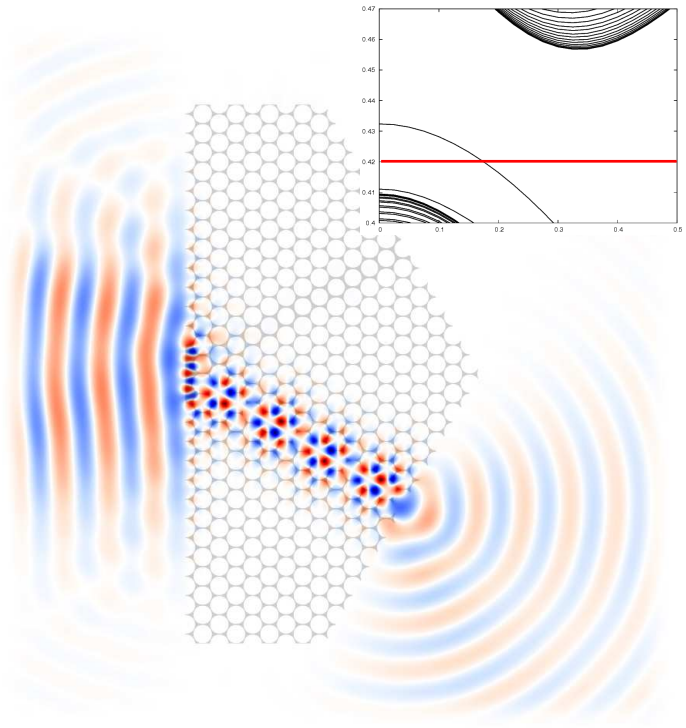

(a)

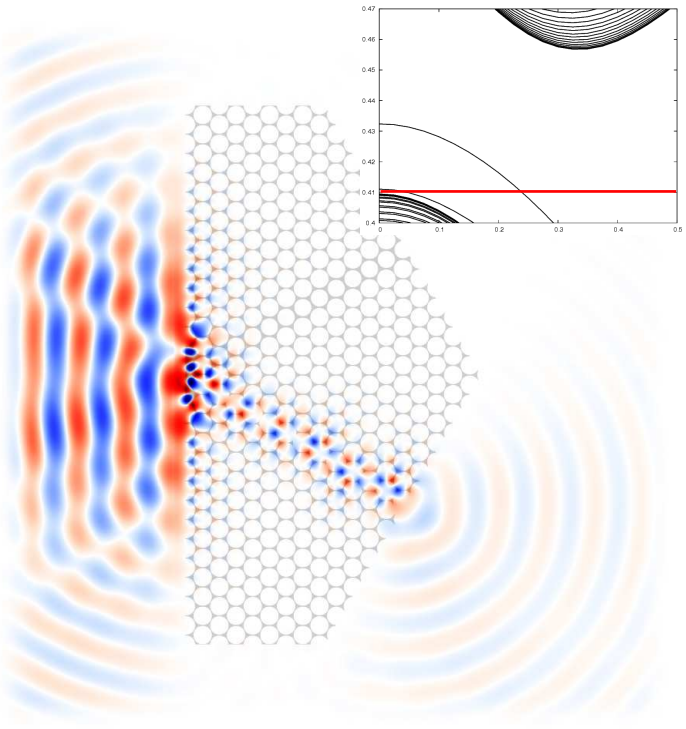

(b)

Figure 3.18. FDTD simulation for (a) $w = 0.420$ and (b) $w = 0.410$. EM waves are splitted very well with the PhC waveguide-2.

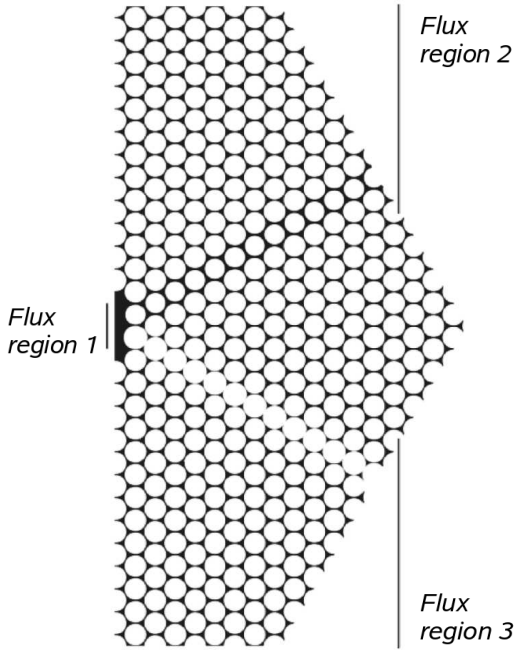

(a)

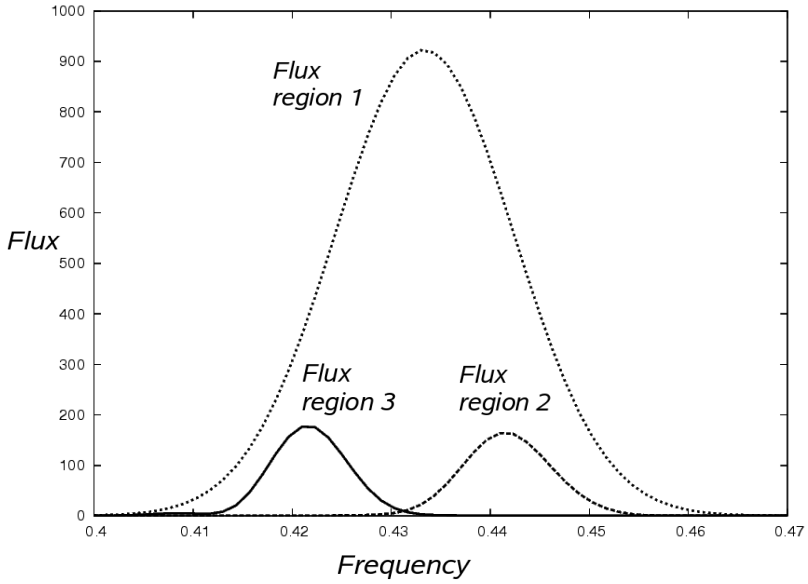

(b)

Figure 3.19. (a) The flux regions for flux measurements. The flux region-1 is for incident EM waves. The flux region-2 and the flux region-3 are for transmitted EM waves. (b) A flux measurement for a Gaussian source $w = 0.433$ with a Gaussian width $\Delta w = 0.040$. The PhC demultiplexer splits the Gaussian signal in frequency axis into two Gaussian signals, which are roughly $w = 0.442$ with $\Delta w = 0.025$ for the flux region-2 and $w = 0.422$ with $\Delta w = 0.025$ for the flux region-3.

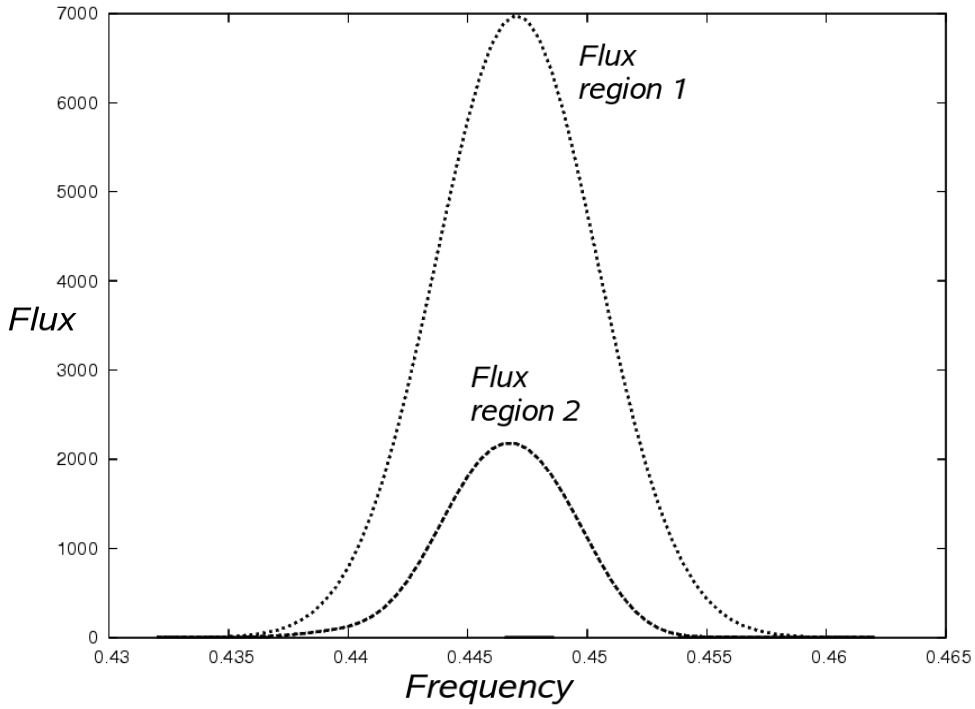

(a)

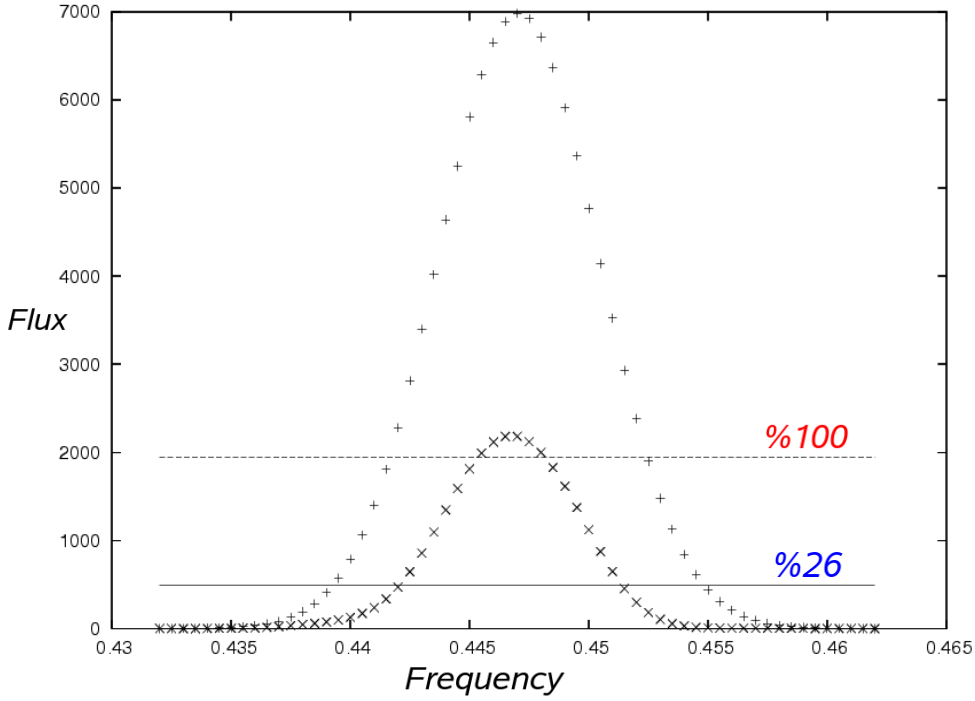

(b)

Figure 3.20. (a) A flux measurement for the PhC waveguide-1, where the Gaussian source is $w = 0.447$ with a Gaussian width $\Delta w = 0.015$. (b) By using mean value theorem, we calculate a transmission of $\%26$ for the PhC waveguide-1.

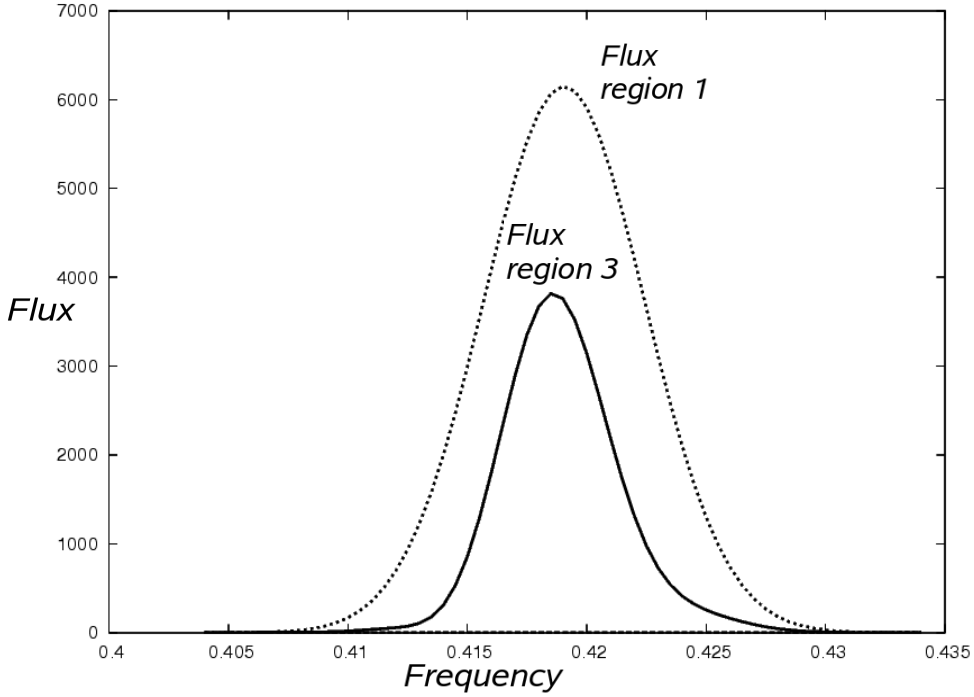

(a)

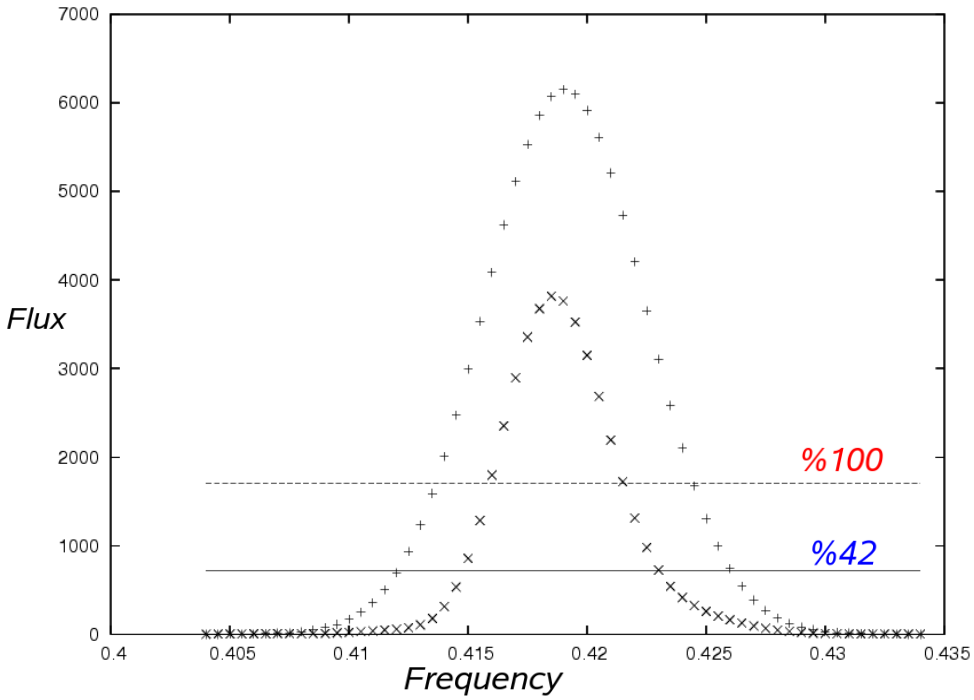

(b)

Figure 3.21. (a) A flux measurement for the PhC waveguide-2, where the Gaussian source is $w = 0.419$ with a Gaussian width $\Delta w = \Delta w = 0.015$. (b) With mean value theorem, we calculate a transmission of $\%42$ for the PhC waveguide-2.

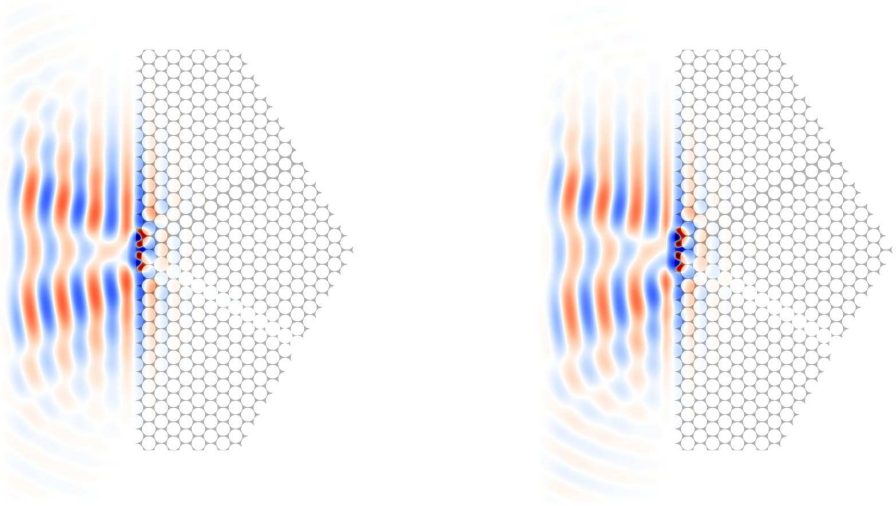

(a) (b)

Figure 3.22. FDTD simulation for (a) $w = 0.453$, (b) $w = 0.448$. TM modes are reflected by the splitting device.

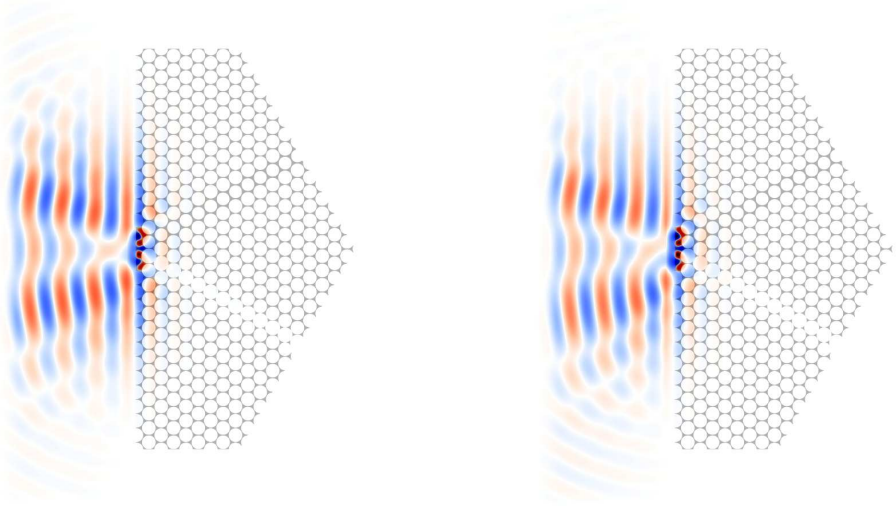

(a) (b)

Figure 3.23. FDTD simulation for (a) $w = 0.443$ and (b) $w = 0.438$. TM modes are reflected by the splitting device.

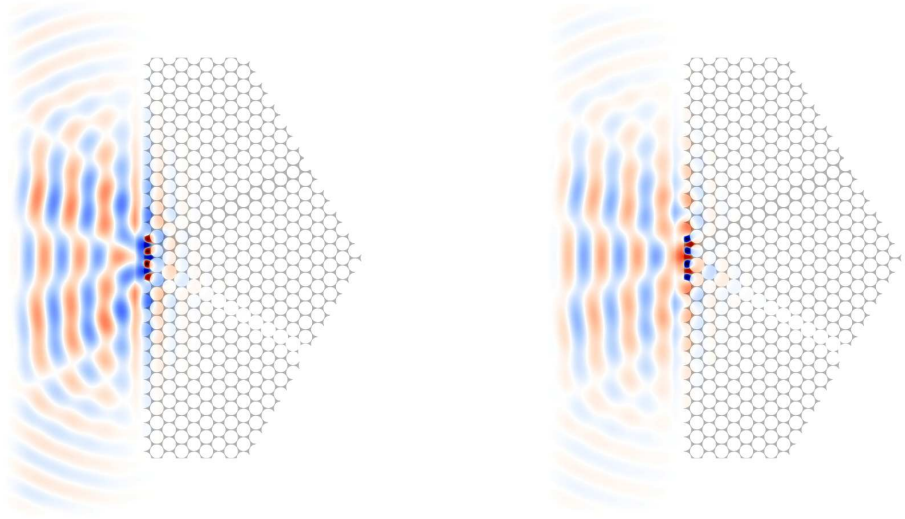

(a) (b)

Figure 3.24. FDTD simulation for (a) $w = 0.428$, (b) $w = 0.423$. TM modes are reflected by the splitting device.

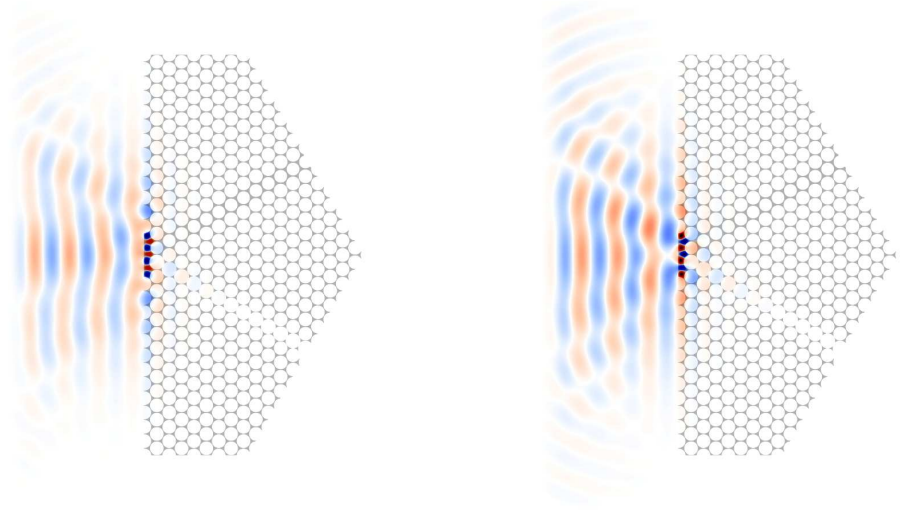

(a) (b)

Figure 3.25. FDTD simulation for (a) $w = 0.417$ and (b) $w = 0.412$. TM modes are reflected by the splitting device.

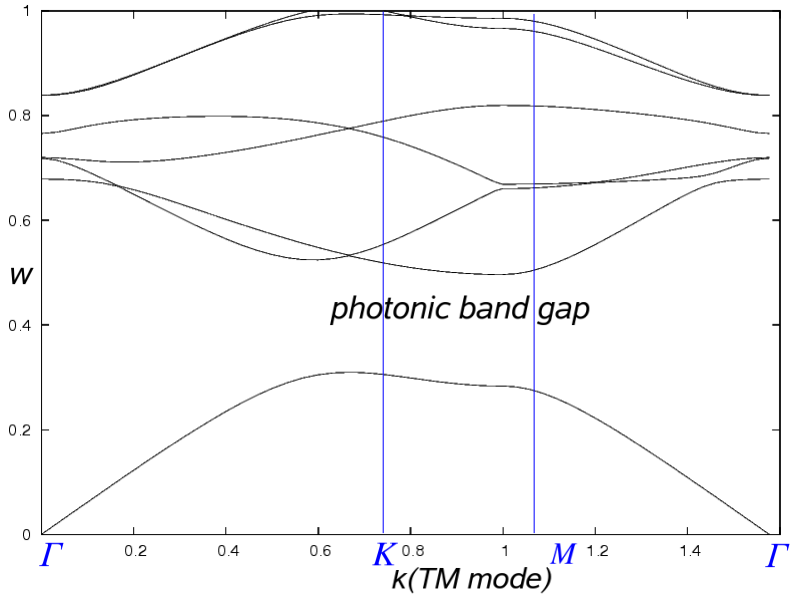

Figure 3.26. The band structure of TM modes for the used PhC. There is a band gap between $0.31 < w < 0.49$.

The flux, which we mean in the title, is

$$\Phi = \int_{flux\ region} \mathbf{S} \cdot d\mathbf{a} \tag{3.2}$$

There are 3 flux regions for flux measurements in Figure 3.19a. The flux region-1 is for incident EM waves. The flux region-2 and region-3 are for transmitted EM waves. A flux measurement for a Gaussian source $w = 0.433$ with a Gaussian width $\Delta w = 0.040$ is in Figure 3.19b. The PhC demultiplexer splits the Gaussian signal in frequency axis into two Gaussian signals, which are roughly $w = 0.442$ with $\Delta w = 0.025$ for the flux region-2 and $w = 0.422$ with $\Delta w = 0.025$ for the flux region-3.

A flux measurement for the PhC waveguide-1 in the PhC demultiplexer in Figure 3.20a, where we use a Gaussian source $w = 0.447$ with a Gaussian width $\Delta w = 0.015$. By using mean value theorem, we calculate a transmission of $\%26$ (see Figure 3.20b).

A flux measurement for the PhC waveguide-2 in the PhC demultiplexer in Figure 3.21a, where we use a Gaussian source $w = 0.419$ with a Gaussian width $\Delta w = 0.015$. With mean value theorem, we calculate a transmission of $\%42$ in Figure 3.21b. The transmission of the PhC waveguide-1 is higher than the transmission of the PhC waveguide-2.

3.5. TM modes

Our calculations are for only TE modes. *Then how does our PhC demultiplexer behave for TM modes?* FDTD results for TM modes in Figure 3.22-3.24. Our frequency splitting device behaves like a reflector for TM modes at all frequencies between $0.412 \leq w \leq 0.453$.

The band structure of TM modes for the used PhC (see Figure 3.1) is in Figure 3.26. The photonic band gap ($0.31 < w < 0.49$) for TM modes covers the photonic band gap ($0.410 < w < 0.456$) for TE modes.

CHAPTER 4

CONCLUSION

According to the results we say that our frequency splitting device can separate different frequencies for TE modes. However the device behaves like a reflector for TM modes. We have used the dimensionless frequency range $0.410 < w < 0.456$. In addition our calculations are for visible light range of EM spectrum since we have taken $\epsilon_{diel} = 11.7$ for visible spectrum. So we can take that the middle frequency $w = 0.433$ of the used range is orange light 496 THz, where the orange range is 484 THz $< w' <$ 508 THz. Then the used range becomes 469 THz $< w' <$ 522 THz in EM wave spectrum. The red and yellow ranges are 400 THz $< w' <$ 484 THz and 508 THz $< w' <$ 526 THz. Therefore the used range contains red, orange and yellow light. *If a source, which contains red, orange and yellow light, comes the frequency splitting device, what will happen?* According to our estimation in the thesis, red and yellow light will be splitted apart (see Figure 4.1a).

What is the size of the PhC demultiplexer? When $w = 0.433$ and $w' = 496$ THz are used in

$$\frac{w'a}{2\pi c} = w \tag{4.1}$$

we find $a = 1.646\mu m$. So our device size equals to $28a = 46\mu m$. Its input size is $2a = 3.3\mu m$.

Where is the PhC demultiplexer used? As we said in Section 1.3, (de)multiplexers are used for splitting the signals apart to deals with a multiplication in capacity for communications. With our device, the capacity in optical fiber technology can be made double or more. A core diameter, which carries signals, is $8\mu m$ for a typical fiber. So the input size of our device is appropriate with the core size (see Figure 4.1b).

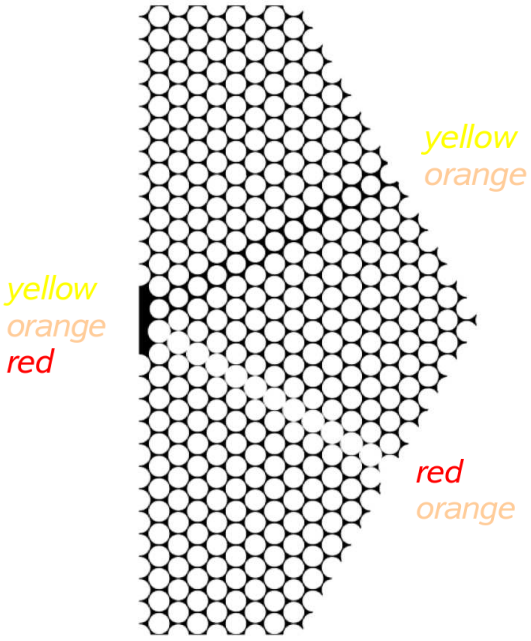

(a)

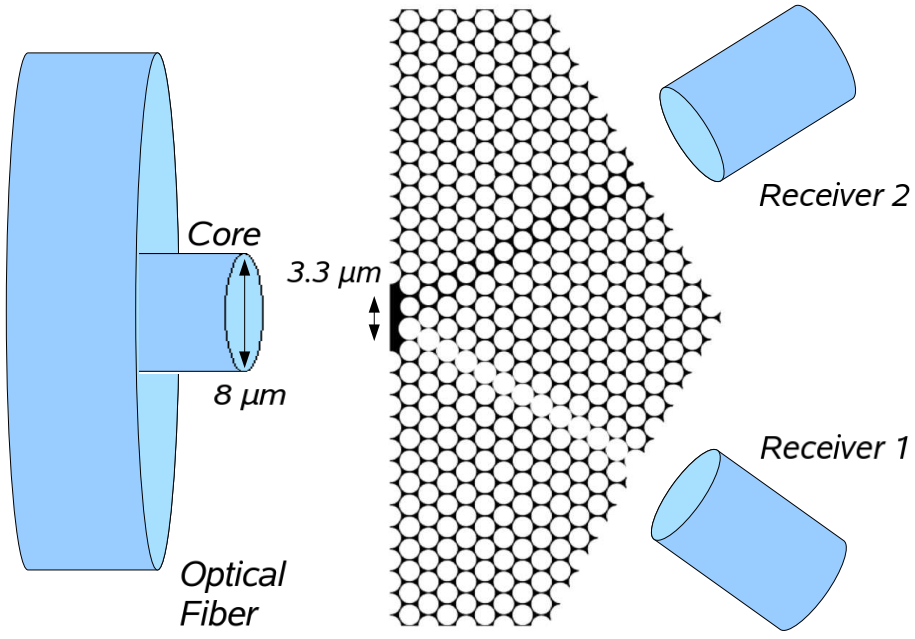

(b)

Figure 4.1. (a) A source, which contains red, orange and yellow light, comes the frequency splitting device. Red and yellow light are splitted apart. (b) A symbolic illustration for an optical communication application of our PhC demultiplexer. The PhC demultiplexer makes the capacity of the fiber optic double.

REFERENCES

Anderson, E., Z. Bai, C. Bischof, S. Blackford, J. Demmel, J. Dongarra, J. Du Croz, A. Greenbaum, S. Hammarling, A. McKenney, D. Sorensen, 1999. *Lapack Users' Guide*. Philadelphia: Society for Industrial and Applied Mathematics.

Arfken, George B. and Hans J. Weber. 2005. *Mathematical Methods for Physicists.* Massachusetts: Elsevier Academic Press.

Berenger, J. P. 1994. A Perfectly Matched Layer for the Absorption of Electromagnetic Waves. *Journal of computational physics* 114:185-200.

Birks, T. A., J. C. Knight, P. S. J. Russell, 1997. Endlessly Singlemode Photonic Crystal Fiber. *Optics Letters* 22:961-63.

Centeno, E., B. Guizal, D. Felbacq, 1999. Multiplexing and Demultiplexing with Photonic Crystals. *Journal of Optics A: Pure and Applied Optics* 1:L10.

Chien, F. S. S., Y. J. Hsu, W. F. Hsieh, S. C. Cheng, 1999. Dual Wavelength Demultiplexing by Coupling and Decoupling of Photonic Crystal Waveguides. *Progress in Quantum Electronics* 12:1119.

Chung, K. B., S. W. Hong, 2002. Wavelength Demultiplexers Based on the Superprism Phenomena in Photonic Crystals. *Applied Physics Letters* 81:1549-51.

Cregan, R. F., B. J. Mangan, J. C. Knight, T. A. Birks, P. S. J. Russell, P. J. Roberts, D. C. Allan, 1999. Single-Mode Photonic Band Gap Guidance of Light in Air. *Science* 285:1537-39.

Fan, S., P. R. Villeneuve, J. D. Joannopoulos, E. F. Schubert, 1997. High Extraction Efficiency of Spontaneous Emission from Slabs of Photonic Crystals. *Physical Review Letters* 78:3294-97.

Fan, S., P. R. Villeneuve, J. D. Joannopoulos, H. A. Haus, 1998. Channel Drop Tunneling through Localized States. *Physical Review Letters* 80:960-63.

Fan, S., S. G. Johnson, J. D. Joannopoulos, C. Manolatou, H. A. Haus, 2001. Waveguide Branches in Photonic Crystals. *Journal of the Optical Society of America B* 18:162-65.

Fink, Y., J. N. Winn, S. Fan, C. Chen, J. Michel, J. D. Joannopoulos, E. L. Thomas, 1998. A Dielectric Omnidirectional Reflector. *Science* 282:1679-82.

Foresi, J. S., P. R. Villeneuve, J. Ferrera, E. R. Thoen, G. Steinmeyer, S. Fan, J. D. Joannopoulos, L. C. Kimerling, H. I. Smith, E. P. Ippen, 1997. Photonic-Bandgap Microcavities in Optical Waveguides. *Nature* 390:143-45.

Griffiths, David. 1999. *Introduction to Electrodynamics.* New Jersey: Prentice Hall.

Ho, K. M., C. T. Chan, C. M. Soukoulis, 1990. Existence of a Photonic Gap in Periodic Dielectric Structures. *Physical Review Letters* 65:3152.

Joannopoulos, John D., Steven G. Johnson, Joshua N. Winn, Robert D. Meade, 2008. *Photonic Crystals: Molding the Flow of Light.* New Jersey: Princeton University Press.

John, S. 1987. Strong Localization of Photons in Certain Disordered Dielectric Superlattices. *Physical Review Letters* 58:2486-89.

Kittel, Charles. 1996. *Introduction to Solid State Physics.* New York: John Wiley.

Knight, J. C., T. A. Birks, P. S. J. Russell, D. M. Atkin, 1996. All-Silica Single-Mode Optical Fiber with Photonic Crystal Cladding. *Optics Letters* 21:1547-49.

Knight, J. C., J. Broeng, T. A. Birks, P. S. J. Russell, 1998. Photonic Band Gap Guidance in Optical Fibers. *Science* 282:1476-78.

Kosaka, H., T. Kawashima, A. Tomita, M. Notomi, T. Tamamura, T. Sato, S. Kawakami, 1998. Superprism Phenomena in Photonic Crystals. *Physical Review B* 58:R10 096-99.

Kosaka, H., T. Kawashima, A. Tomita, M. Notomi, T. Tamamura, T. Sato, S. Kawakami, 1999. Self-Collimating Phenomena in Photonic Crystals. *Applied Physics Letters* 74:1212-14.

Koshiba, M. 2001. Wavelength Division Multiplexing and Demultiplexing with Photonic Crystal Waveguide Couplers. *Journal of Lightwave Technology* 19:1970.

Lin, S. Y., E. Chow, V. Hietala, P. R. Villeneuve, J. D. Joannopoulos, 1998. Experimental Demonstration of Guiding and Bending of Electromagnetic Waves in a Photonic Crystal. *Science* 282:274-76.

Lin, S. Y., E. Chow, J. Bur, S. G. Johnson, J. D. Joannopoulos, 2002. Low-Loss, Wide Angle Y Splitter at $\sim$1.6-mm Wavelengths Built with a Two Dimensional Photonic Crystal. *Optics Letters* 27:1400-02.

Loncar, M., T. Yoshie, A. Scherer, P. Gogna, Y. Qiu, 2002. Low-Threshold Photonic Crystal Laser. *Applied Physics Letters* 81:2680-82.

Luo, C., S. G. Johnson, J. D. Joannopoulos, J. B. Pendry, 2002. All-Angle Negative Refraction without Negative Effective Index. *Physical Review B* 65:201104-1-4.

Matsumoto, T., S. Fujita, T. Baba, 2005. Wavelength Demultiplexer Consisting of Photonic Crystal Superprism and Superlens. *Optics Express* 13:10768-76.

Meade, R. D., K. D. Brommer, A. M. Rappe, J. D. Joannopoulos, 1991. Photonic Bound States in Periodic Dielectric Materials. *Physical Review B* 44:13772.

Meade, R. D., K. D. Brommer, A. M. Rappe, J. D. Joannopoulos, 1992. Existence of a Photonic Band Gap in Two Dimensions. *Applied Physics Letters* 61:495.

Meade, R. D., A. M. Rappe, K. D. Brommer, J. D. Joannopoulos, O. L. Alerhand, 1993. Accurate Theoretical Analysis of Photonic Band-Gap Materials. *Physical Review B* 48:8434.

Mekis, A., J. C. Chen, I. Kurland, S. Fan, P. R. Villeneuve, J. D. Joannopoulos, 1996. High Transmission through Sharp Bends in Photonic Crystal Waveguides. *Physical Review Letters* 77:3787-90.

Momeni, B., A. Adibi, 2003. Optimization of Photonic Crystal Demultiplexers Based on the Superprism Effect. *Applied Physics B: Lasers and Optics* 77:555-60.

Momeni, B., J. Huang, M. Soltani, M. Askari, S. Mohammadi, M. Rakhshandehroo, A. Adibi, 2006. Compact Wavelength Demultiplexing Using Focusing Negative Index Photonic Crystal Superprisms. *Optics Express* 14:2413.

Nelson, B. E., M. Gerken, D. A. Miller, R. Piestun, C. C. Lin, J. S. Harris, 2000. Use of a Dielectric Stack as a One-Dimensional Photonic Crystal for Wavelength Demultiplexing by Beam Shifting. *Optics Express* 25:1502.

Notomi, M. 2000. Theory of Light Propagation in Strongly Modulated Photonic Crystals: Refractionlike Behavior in the Vicinity of the Photonic Band Gap. *Physical Review B* 62:10 696-705.

Notomi, M., S. Akihiko, S. Mitsugi, G. Kira, E. Kuramochi, T. Tanabe, 2005. Optical Bistable Switching Action of Si High-Q Photonic-Crystal Nanocavities. *Optics Express* 13:2678-87.

Park, H. G., S. H. Kim, S. H. Kwon, Y. G. Ju, J. K. Yang, J. H. Baek, S. B. Kim, Y. H. Lee, 2004. Electrically Driven Single Cell Photonic Crystal Laser. *Science* 305:1444-47.

Plihal, M., A. A. Maradudin, 1991. Photonic Band Structure of Two-Dimensional Systems: The Triangular Lattice. *Physical Review B* 44:8565.

Russell, P. S. J. 2006. Photonic-Crystal Fibers. *Journal of Lightwave Technology* 24:4729-49.

Satpathy, S., Z. Zhang, M. R. Salehpour, 1990. Theory of Photon Bands in Three Dimensional Periodic Dielectric Structures. *Physical Review Letters* 65:2478.

Sharkawy, A., S. Shi, D. W. Prather, 2001. Multichannel Wavelength Division Multiplexing with Photonic Crystals. *Applied Optics* 40:2247.

Smajic, J., C. Hafner, D. Erni, 2003. On the Design of Photonic Crystal Multiplexers. *Optics Express* 11:566.

Sözüer, H. S., J. W. Haus, R. Inguva, 1991. Photonic Bands: Convergence Problems with the Plane Wave Method. *Physical Review B* 45:13962.

Sözüer, Sami H. 2009. Lecture Notes on Photonic Structures.

Taflove, A., M. E. Brodwin, 1975. Numerical Solution of Steady-State Electromagnetic Scattering Problems Using the Time-Dependent Maxwell's Equations. *IEEE Transactions on Microwave Theory and Techniques* 23:623.

Villeneuve, P. R., S. Fan, J. D. Joannopoulos, 1996. Microcavities in Photonic Crystals: Mode Symmetry, Tunability, and Coupling Efficiency. *Physical Review B* 54:7837-42.

Yablonovitch, E. 1987. Inhibited Spontaneous Emission in Solid State Physics and Electronics. *Physical Review Letters* 58:2059-62.

Yanık, M. F., S. Fan, M. Soljačić, J. D. Joannopoulos, 2003. All Optical Transistor Action with Bistable Switching in a Photonic Crystal Cross-Waveguide Geometry. *Optics Letters* 28:2506-08.

Yee, K. S. 1966. Numerical Solution of Initial Boundary Value Problems Involving Maxwell's Equations in Isotropic Media. *IEEE Transactions on Antennas and Propagation* 14:302.

Zhang, Z., S. Satpathy 1990. Electromagnetic Wave Propagation in Periodic Structures: Bloch Wave Solution of Maxwells Equations. *Physical Review Letters* 65:2650.